

1 **The life cycle of Northern Hemisphere downward wave coupling**  
2 **between the stratosphere and troposphere**

3 **TIFFANY A. SHAW** \*

*Department of Earth and Environmental Sciences &*

*Department of Applied Physics and Applied Mathematics,*

*Columbia University, New York, New York, USA*

4 **JUDITH PERLWITZ** †

*Cooperative Institute for Research in Environmental Sciences, University of Colorado, Boulder, Colorado, USA*

---

\* *Corresponding author address:* Dr. Tiffany A. Shaw, Department of Earth and Environmental Sciences and Department of Applied Physics and Applied Mathematics, Columbia University, P.O. Box 1000, 61 Route 9W, Palisades, NY, 10964, E-mail: tas2163@columbia.edu

†Also at: NOAA/Earth System Research Laboratory, Physical Sciences Division, Boulder, Colorado

## ABSTRACT

5  
6 The life cycle of Northern Hemisphere downward wave coupling between the stratosphere  
7 and troposphere via wave reflection is analyzed. Wave reflection events are defined by ex-  
8 treme negative values of a wave-coupling index based on the leading principal component  
9 of the daily wave-1 heat flux at 30 hPa. The life cycle occurs over a 28-day period. In the  
10 stratosphere there is a transition from positive to negative total wave-1 heat flux and west-  
11 ward to eastward phase tilt with height of the wave-1 geopotential height field. In addition,  
12 the zonal-mean zonal wind in the upper stratosphere weakens leading to negative vertical  
13 shear.

14 Following the evolution in the stratosphere there is a shift toward the positive phase  
15 of the North Atlantic Oscillation (NAO) in the troposphere. The pattern develops from a  
16 large westward propagating wave-1 anomaly in the high-latitude North Atlantic sector. The  
17 subsequent equatorward propagation leads to a positive anomaly in midlatitudes. The near  
18 surface temperature and circulation anomalies are consistent with a positive NAO phase.  
19 The results suggest that wave reflection events can directly influence tropospheric weather.

20 Finally, winter seasons dominated by extreme wave coupling and stratospheric vortex  
21 events are compared. The largest impacts in the troposphere occur during the extreme  
22 negative seasons for both indices, namely seasons with multiple wave reflection events lead-  
23 ing to a positive NAO phase or seasons with major sudden stratospheric warmings (weak  
24 vortex) leading to a negative NAO phase. The results reveal that dynamical coupling be-  
25 tween the stratosphere and NAO involves distinct dynamical mechanisms that can only be  
26 characterized by separate wave-coupling and zonal indices.

# 27 1. Introduction

28 Dynamical coupling between the stratosphere and troposphere is a key component of  
29 atmospheric variability in the winter hemisphere. Understanding the mechanisms involved  
30 in the coupling and their impact on tropospheric weather and climate is an important topic  
31 of current research (Shaw and Shepherd 2008; Gerber et al. 2012). It is well known that  
32 stratosphere-troposphere coupling is driven by the upward propagation of planetary scale  
33 waves generated in the troposphere. A significant amount of research has been focused on  
34 understanding the coupling during weak stratospheric vortex events, e.g. sudden strato-  
35 spheric warming events, that involve the absorption of wave activity in the stratosphere  
36 and the downward migration of zonal-mean zonal-wind and temperature anomalies (e.g.  
37 Baldwin and Dunkerton 1999, 2001; Christiansen 2001; Plumb and Semeniuk 2003). When  
38 the zonal-mean anomalies reach the lower stratosphere/upper troposphere they can initiate  
39 baroclinic eddy responses that subsequently produce anomalies in the tropospheric circu-  
40 lation, e.g. meridional shifts of the jet, that can be maintained by eddy feedbacks (e.g.  
41 Polvani and Kushner 2002; Song and Robinson 2004; Limpasuvan et al. 2004) and produce  
42 surface temperature and mean sea level pressure anomalies. In addition, weak vortex events  
43 produce potential vorticity anomalies in the stratosphere that can directly impact the tropo-  
44 sphere via hydrostatic and geostrophic adjustment (Hartley et al. 1998; Black 2002; Ambaum  
45 and Hoskins 2002). Baldwin and Dunkerton (2001) showed that strong stratospheric vor-  
46 tex events can also impact the troposphere. Polar vortex intensification is accompanied by  
47 equatorward propagation of wave activity in the stratosphere (Hartmann et al. 2000) with  
48 the impacts in the troposphere resulting from the subsequent hydrostatic and geostrophic  
49 adjustment of the vortex (Ambaum and Hoskins 2002).

50 In addition to coupling involving weak and strong vortex states, Perlwitz and Harnik  
51 (2003, 2004) and Shaw et al. (2010) showed that wave reflection in the stratosphere can  
52 impact the tropospheric wave structure, a process called “downward wave coupling”. Shaw  
53 et al. (2010), hereafter SPH10, used the statistical cross-correlation technique employed by

54 Randel (1987) to show that upward wave-1 coupling from 500 to 30 hPa occurs over a 5-  
55 day period and is followed by downward wave-1 coupling from 30 to 500 hPa over a 5-day  
56 period. In the Northern Hemisphere, downward wave coupling maximized during January,  
57 February and March (JFM). Note that the wave-coupling time scales are much shorter than  
58 timescales associated with the downward migration of zonal-mean anomalies during extreme  
59 vortex events. SPH10 showed that downward wave-1 coupling is associated with a particular  
60 configuration of the stratospheric basic state that is favorable for wave-1 reflection in the  
61 stratosphere. The basic state configuration involves a meridional wave evanescence region in  
62 the subtropical stratosphere and a vertical wave evanescence region in the upper stratosphere  
63 (SPH10). The vertical wave evanescence coincides with a region of negative vertical zonal-  
64 wind shear (Perlwitz and Harnik 2003, 2004) whereas the meridional wave evanescence region  
65 is associated with negative meridional zonal-wind shear. The configuration channels wave  
66 activity upward from the troposphere to the stratosphere and upon wave reflection from the  
67 stratosphere to the troposphere. Perlwitz and Harnik (2004) showed that individual winters  
68 in the Northern Hemisphere could be characterized as being dominated by wave reflection  
69 or wave absorption type stratosphere-troposphere coupling, each type being associated with  
70 distinct stratospheric basic states.

71 All stratosphere-troposphere coupling events, whether they involve anomalous vortex  
72 states or downward wave coupling, originate as events of upward wave propagation (upward  
73 wave coupling) events from the troposphere (Haynes 2005). Polvani and Waugh (2004) and  
74 Limpasuvan et al. (2004) showed that weak vortex events were preceded by anomalous pos-  
75 itive 40-day, 45 to 75°N averaged 100 hPa (meridional) heat flux events that were extreme  
76 (far from the mean). They argued that weak vortex events are “true events” because they  
77 were associated with extreme positive heat flux events, i.e. enhanced propagation of plane-  
78 tary wave activity into the stratosphere. In contrast, the relationship between strong vortex  
79 and heat flux events is less clear. Polvani and Waugh (2004) showed that strong vortex  
80 events were associated with anomalous weakly negative 40-day, 45 to 75°N averaged 100

81 hPa heat flux (see their Fig. 1). However, an anomalous negative heat flux event is not  
82 associated with a distinct dynamical mechanism since it can imply either weakened upward  
83 wave coupling or downward wave coupling (i.e. wave reflection). The latter occurs if the  
84 total (climatology plus anomaly) heat flux is negative because the total heat flux is pro-  
85 portional to the vertical group velocity. Recall that the meridional heat flux contributes  
86 to the vertical Eliassen-Palm flux, which is equal to the vertical group velocity times the  
87 wave-activity density in the quasi-geostrophic and small-amplitude limits. The relationship  
88 between negative total heat flux events and strong vortex events has not been investigated  
89 previously. A complete characterization of stratosphere-troposphere coupling requires a bet-  
90 ter understanding of negative heat flux events, their relationship to vortex events, and their  
91 impact on the troposphere.

92 Here we use the daily wave-1 heat flux to isolate and analyze downward wave coupling  
93 events during JFM in the Northern Hemisphere. The events are defined by extreme negative  
94 values of a daily wave-coupling index equal to the standardized principal component (pc)  
95 of the leading empirical orthogonal function (EOF) of the wave-1 heat flux. The pc time  
96 series is utilized instead of the daily heat flux anomaly averaged over a specified latitudinal  
97 band, e.g. 45 to 75°N as in Newman et al. (2001) and Polvani and Waugh (2004), because  
98 it encodes the spatial variability via the EOF and the temporal variability via the pc. Note  
99 also that we use a daily index instead of a time-integrated index as in Polvani and Waugh  
100 (2004) because the upward and downward wave coupling processes involve short timescales.

101 Section 2 discusses the data and analysis methods. Section 3 discusses the composite life  
102 cycle of downward wave coupling events in the stratosphere and their impact on tropospheric  
103 weather. In addition, the seasonal impacts of downward wave coupling on the troposphere  
104 and the relationship to the conventional weak/strong vortex paradigms of stratosphere-  
105 troposphere coupling is analyzed. The results are summarized and discussed in section 4.

## 2. Data and event definition

The data used in this study are the daily three-dimensional zonal and meridional wind, temperature, and geopotential height from the European Centre for Medium-Range Weather Forecasts (ECMWF) Interim (ERA-Interim) data set from 1979 to 2011 (Dee et al. 2011). The data are provided on 37 pressure levels with a horizontal resolution of  $1.5^\circ$ .

The focus of the analysis is on downward wave coupling associated with planetary waves with zonal wave number 1 (downward wave-1 coupling). SPH10 showed that downward wave-1 coupling maximizes during JFM. Downward wave-2 coupling also occurs in the Northern Hemisphere but it is less frequent (SPH10) and consequently it is more difficult to quantify its impact on the troposphere based on a record as short as the ERA-Interim data set.

The life cycle analysis is based on the pc of the leading EOF of the zonal-mean wave-1 heat flux at 30 hPa in the Northern Hemisphere. The 30 hPa level is chosen so that the cause of downward wave coupling events can be clearly attributed to events originating in the stratosphere. The leading EOF is calculated using the entire 12045-day time series (365 days and 33 years) from 20 to  $90^\circ\text{N}$  with a meridional weighting following Baldwin et al. (2009). The leading EOF explains 84% of the total variance and is well separated from higher modes according to the criterion of North et al. (1982). The magnitude of the pc, which is defined over the whole year, is largest during winter consistent with vertical planetary wave propagation during winter. As a result, the standard deviation of the pc during JFM is  $\sigma_{JFM} = 1.7$ , which is larger than the standard deviation for all days, e.g.  $\sigma = 1.0$  (as per the definition from the EOF analysis).

The climatological JFM wave-1 heat flux is positive from the surface to the upper stratosphere (Fig. 1, top-left panel) and suggests that the climatology is dominated by upward wave propagation, which is consistent with SPH10 who showed that downward wave coupling occurs as part of the intraseasonal variability. Figure 1 (top-middle panel) shows the leading spatial pattern of variability of wave-1 heat flux determined by regressing the wave-1 heat flux anomalies at all levels on the standardized 30 hPa pc time series. This heat flux

133 pattern is shifted toward high latitudes relative to the climatology and exhibits a dipole  
134 pattern in the vertical. It is positive in the stratosphere and negative in the troposphere.  
135 The goal of this study is isolate downward coupling events, i.e. time periods when the total  
136 heat flux values in high latitudes is negative indicating a downward group velocity. A pc  
137 value equal to  $-\sigma_{JFM}$  is sufficient to produce a total negative heat flux, e.g. the sum of  
138 the climatological heat flux pattern and  $-\sigma_{JFM}$  times the regression pattern is negative in  
139 high latitudes (Fig. 1, top-right panel). Thus, an extreme pc value of  $-\sigma_{JFM}$  can be used  
140 as a threshold for downward wave coupling events. The histogram of JFM pc values (Fig.  
141 1, bottom panel) illustrates that downward wave coupling events are fairly common: the  
142 number of JFM days from 1979 to 2011 with a pc value  $< -\sigma_{JFM}$  ( $> +\sigma_{JFM}$ ) is 332 (418).

143 In order to create a composite life cycle of downward wave coupling we define events  
144 based on a wave-coupling index equal to the 5-day smoothed leading pc time series of daily  
145 heat flux anomalies at 30 hPa. The smoothing allows for a clear assessment of the central  
146 dates of the events. An individual downward wave-coupling event is identified during a given  
147 JFM season when the minimum value of the wave-coupling index during the season is less  
148 than or equal to  $-1.5 \sigma_{JFM}$ . Note that this threshold ensure that the event represents an  
149 extreme value of the pc during JFM and a negative total heat flux in high latitudes at 30  
150 hPa (see Fig. 1, top-right panel). In addition, the event must last at least 5 days, e.g. the  
151 index must be less than  $\sigma_{JFM}$  for 2 days before and after the event, and the index value of  
152 the wave-1 heat flux anomaly time series projected onto the regression pattern at 100 hPa  
153 must be less than  $\sigma_{JFM}$  sometime 5 days following the event. The central date of the event  
154 (day 0) is defined by the day that the index crosses  $-1.0$ . Events defined using the pc at 50  
155 hPa and 100 hPa exhibit similar qualitative behavior as those defined at 30 hPa.

### 3. Results

According to the criteria of section 2, 14 downward wave coupling events occurred during the 33 JFM seasons from 1979 to 2011. The central dates of the individual events are listed in Table 1 along with the minimum total wave-1 heat flux from 40 to 90°N during the event. The life cycle of the composite event is divided into four 7-day stages; stage 1 (-12 to -6 days), stage 2 (-5 to +1 days), stage 3 (2 to 8 days) and stage 4 (9 to 15 days). A 5-day smoothing is applied to all data. The lifecycle approach is similar to Limpasuvan et al. (2004) who studied the life cycle of Northern Hemisphere sudden stratospheric warming events, however the time scale of the stages is much shorter here (7 days versus 15 days in Limpasuvan et al. 2004). Note that the sudden warming events were defined using a stratospheric zonal index based on the 15-day low pass filtered leading pc time series of daily zonal-mean zonal wind anomalies at 50 hPa.

#### *a. Evolution in the stratosphere*

Figure 2 (top) shows the evolution of the wave-1 heat flux anomaly projected onto the regression pattern in Fig. 1 (middle) during the composite downward wave coupling event as a function of time from -15 to 15 days and height. Note that the evolution at 30 hPa is equal to the wave-coupling index, e.g. the leading pc at 30 hPa. The shading indicates statistically significant signals at the 95% level based on a t-test. Figure 2 also shows the time-averaged zonal-mean wave-1 heat flux (middle) and meridional momentum flux (bottom) anomalies during the four stages.

During the first stage the wave-coupling index and heat flux anomaly in the stratosphere are positive and statistically significant. The heat flux anomaly maximum moves from 200 to 10 hPa during the stage, which is indicative of an upward wave coupling precursor. The heat flux anomaly in the troposphere and the momentum flux anomaly throughout the atmosphere are not statistically significant during this stage. During the second stage the wave-coupling index and heat flux anomaly change sign from positive to negative in the mid-

182 to-lower stratosphere in high latitudes. In addition, a positive heat flux anomaly develops in  
183 the troposphere. The vertical dipole of the heat flux is reminiscent of the regression pattern  
184 in Fig. 1 (middle). The momentum flux anomaly exhibits a meridional dipole in the upper  
185 stratosphere. During the third stage the wave-coupling index decreases significantly in the  
186 stratosphere and reaches a minimum value of -3.1 at 30 hPa on day +3. In addition, there  
187 is a statistically significant positive heat flux anomaly in the troposphere. The tropospheric  
188 maximum clearly lags the minimum in the stratosphere. The momentum flux anomaly  
189 exhibits a vertical dipole with a statistically significant negative signal in the troposphere.  
190 Finally during the fourth stage the wave-coupling index and heat flux anomaly weaken but  
191 remain negative in the stratosphere. The heat flux anomaly in the troposphere weakens  
192 significantly and is no longer statistically significant in high latitudes. In contrast, the  
193 momentum flux anomaly in the troposphere and stratosphere remain large.

194 The downward wave coupling event is associated with a transition of the wave-coupling  
195 index and heat flux anomaly from positive to negative in the stratosphere. Since wave-1 and  
196 the zonal-mean flow are well known to be strongly coupled in the stratosphere we also con-  
197 sider the evolution of the zonal-mean flow during the life cycle. The structure of zonal-mean  
198 flow variability is determined by the leading EOF of zonal-mean geopotential height at each  
199 pressure level, e.g. the Northern Annular Mode. Recall that the sign of the leading pc of  
200 the zonal-mean geopotential height in the stratosphere, called the zonal index, indicates the  
201 strength of the stratospheric polar vortex whereas in the troposphere the zonal index indi-  
202 cates the position of the tropospheric jet. In particular, a positive (negative) index indicates  
203 a strong (weak) stratospheric polar vortex and a poleward (equatorward) shift of the tropo-  
204 spheric jet. Because of the strong relationship between the zonal-mean geopotential height  
205 and zonal-mean zonal wind, we consider the evolution of both the zonal index, represent-  
206 ing the zonal-mean geopotential height, and the zonal-mean zonal-wind anomalies during  
207 the composite downward wave coupling event. Figure 3 shows the composite evolution of  
208 the zonal index (top) and the time-averaged zonal-mean zonal-wind anomaly (bottom) dur-

209 ing the four stages. Note that the time series of the zonal index at each pressure level is  
210 based on the leading pc at that level and is aligned to the central dates of the downward  
211 wave coupling events defined by the wave-coupling index at 30 hPa. The shading indicates  
212 statistically significant signals at the 95% level based on a t-test.

213 During the first stage the zonal index is positive from the lower stratosphere to the sur-  
214 face and negative in the upper stratosphere. In addition, there is a statistically significant  
215 positive zonal-mean zonal-wind anomaly in the polar lower stratosphere/upper troposphere  
216 region and a negative zonal-wind anomaly in the subtropical stratosphere. During the sec-  
217 ond stage the zonal index weakens in the upper stratosphere and reaches a minimum of  $-1.4$   
218 at 1 hPa on day  $-1$ , which is associated with a significant weakening of the polar vortex  
219 in the upper stratosphere. In addition, there is a positive zonal-mean zonal-wind anomaly  
220 in high latitudes. Note that the weakening of the zonal index occurs over a relatively short  
221 timescale ( $<$  a week) compared to the weakening during extreme weak vortex events defined  
222 by a zonal-index threshold of  $-1.5$ , which occur over timescales of weeks to months (Bald-  
223 win and Dunkerton 2001). During the third stage of the event the zonal index reaches a  
224 maximum of  $0.9$  at 100 hPa on day  $+11$ . The zonal-mean zonal-wind anomaly is positive  
225 indicating a strengthening of the polar vortex in the stratosphere and a weakening of the  
226 subtropical jet. The negative to positive transition of the zonal index in the upper and  
227 lower stratosphere between  $-5$  to  $+5$  days is reminiscent of the zonal-mean geostrophic and  
228 hydrostatic adjustment to a potential vorticity anomaly (Black 2002; Ambaum and Hoskins  
229 2002). Finally during the fourth stage the zonal index in the lower stratosphere is posi-  
230 tive and coincides with a positive zonal-mean zonal-wind anomaly indicating a strengthened  
231 polar vortex.

232 The positive to negative heat flux anomaly transition during the second stage occurs as  
233 the zonal index in the upper stratosphere is weakening. In order to fully understand the  
234 evolution of wave-1 and the zonal-mean flow one must consider total fields. As discussed pre-  
235 viously, a negative heat flux anomaly can imply reduced upward wave coupling or downward

236 wave coupling. In particular, reduced upward wave coupling involves a negative anomaly but  
237 a positive total heat flux. In contrast, downward wave coupling involves both a negative heat  
238 flux anomaly and a negative total heat flux, implying a downward vertical group velocity.  
239 Similarly, a negative zonal-mean zonal-wind anomaly does not necessarily imply that the  
240 sign of the zonal-mean zonal wind has changed sign, e.g. from westerly to easterly as it does  
241 during a sudden stratospheric warming event. The structure of the total zonal-mean zonal  
242 wind is also relevant in so far as it acts as a wave guide for wave propagation.

243 Figure 4 shows the total zonal-mean zonal wind, wave-1 meridional heat flux, negative  
244 wave-1 meridional momentum flux and wave-1 geopotential height at  $70^\circ\text{N}$  during the four  
245 stages of the composite downward wave coupling event. The shading in the zonal-mean  
246 zonal-wind panels represents regions of vertical and meridional wave evanescence defined  
247 by negative vertical and meridional wave numbers. The wave numbers are calculated from  
248 the solution to the wave equation associated with the conservation of potential vorticity  
249 in spherical coordinates linearized about a zonal-mean basic state following Harnik and  
250 Lindzen (2001). The regions of vertical and meridional wave evanescence indicate regions  
251 where wave propagation is not permitted according to linear theory. During the first stage  
252 the polar vortex peaks in the upper stratosphere. There is only a small region of vertical  
253 wave evanescence in the upper stratosphere, which is associated with a region of negative  
254 vertical zonal-wind shear. The configuration is very favorable for upward wave coupling as  
255 indicated by the positive total heat flux and the westward phase tilt with height from the  
256 mid-troposphere to the mid-stratosphere. The wave-1 amplitude in the mid troposphere is  
257 weak and the pattern at the surface is out-of-phase with the levels directly above, which is  
258 likely because the wave-1 pattern at the surface is strongly constrained by orography and  
259 ocean-land heating asymmetries. The momentum flux is poleward in the high-latitude upper  
260 troposphere/lower stratosphere and equatorward in the upper stratosphere.

261 During the second stage the maximum zonal-mean zonal wind resides just below 10 hPa  
262 and consequently the region of negative vertical zonal-wind shear and vertical wave evanes-

263 cence extends down to 5 hPa. The descent of the wave evanescence region seems to coincide  
264 with the upward wave coupling precursor. In addition, the latitudinal width of the merid-  
265 ional wave guide becomes narrower during this stage. Overall, the vortex configuration is  
266 very favorable for downward wave coupling because upward propagating waves will almost  
267 certainly encounter the reflecting surface and will be forced to reflect and propagate down-  
268 ward into the troposphere because of the narrow meridional wave guide. There are signs of  
269 the beginning stages of wave reflection in the lower stratosphere where the total heat flux  
270 is negative and the westward phase tilt from the lower-to-upper stratosphere has weakened.  
271 The wave-1 amplitude in the mid troposphere has increased and at the surface appears to  
272 extend into the free troposphere, however this is partly the result of the expansion of the  
273 wave-1 pattern in high latitudes, which cannot be captured by showing the wave pattern at  
274 a single latitude (see Fig. 5, bottom).

275 During the third stage the zonal-mean zonal-wind configuration remains favorable for  
276 wave reflection. The total wave-1 heat flux is negative in the polar upper troposphere/lower  
277 stratosphere to the mid stratosphere and its magnitude is as large as the positive heat flux  
278 during stage one. In addition, the vertical Eliassen-Palm flux is negative in the high-latitude  
279 mid-to-lower stratosphere (not shown) while its vertical divergence is positive (not shown).  
280 The region of negative momentum flux expands poleward suggesting enhanced equatorward  
281 propagation in midlatitudes during this stage (compare with Fig. 2, bottom). The wave  
282 pattern exhibits a clear eastward phase tilt with height from the mid-troposphere to the  
283 mid-stratosphere, which is indicative of wave reflection and downward wave coupling. The  
284 whole wave pattern from the mid troposphere to mid stratosphere has shifted westward and  
285 the wave pattern in the mid-troposphere reaches its maximum amplitude. Finally during the  
286 fourth stage the zonal-mean zonal wind has strengthened in the mid and lower troposphere.  
287 The heat flux is positive throughout the atmosphere and wave-1 exhibits a clear standing  
288 wave pattern in the vertical. The standing wave pattern implies interference between upward  
289 and downward propagating waves. The sign of the heat flux suggests that the upward

290 propagating wave dominates.

291 *b. Impact on the troposphere*

292 Downward wave-1 coupling events clearly coincide with changes in the tropospheric wave  
293 pattern. In particular, there is a pronounced amplification and westward phase shift of the  
294 high latitude wave-1 pattern that occurs as it achieves an eastward phase tilt with height  
295 from the mid-troposphere to the mid-stratosphere (see Fig. 4, bottom). The evolution of  
296 the high-latitude wave-1 pattern can be illustrated using a Hovmöller plot. Figure 5 (top)  
297 shows the total wave-1 pattern averaged from 60 to 80°N at 500 hPa (black contours) and  
298 10 hPa (color) as a function of longitude and time from  $-15$  to  $+15$  days. The longitude-  
299 latitude patterns from 30°N to 90°N at 500 hPa during the four stages are also shown (Fig.  
300 5, bottom). During the first stage the 500 hPa high-latitude wave pattern is very weak  
301 consistent with the climatological pattern at these latitudes. Note however that there is a  
302 robust wave-1 pattern in midlatitudes that is out of phase with the high-latitude wave-1  
303 pattern. During the second stage the amplitude of the 10 hPa high-latitude wave pattern  
304 reaches a maximum and precedes the maximum amplitude at 500 hPa, which occurs during  
305 stage three. The phase tilt with height from 500 and 10 hPa is clearly eastward. The  
306 midlatitude wave-1 pattern at 500 hPa does not exhibit a large change in amplitude or  
307 phase. During this stage the phase of the high-latitude wave-1 pattern at 500 hPa begins to  
308 shift westward, which is consistent with the pattern being synchronized with the levels above.  
309 The amplitude of the high-latitude 500 hPa wave pattern reaches a maximum during the  
310 third stage. At the same time the pattern continues to move westward and by the end of the  
311 stage the phase has moved approximately 120 degrees westward, which implies a phase speed  
312 of approximately  $-2.6 \text{ ms}^{-1}$ . During this stage the high-latitude wave pattern is clearly out  
313 of phase with the midlatitude wave pattern. Finally during the fourth stage the amplitude  
314 of the high latitude wave-1 pattern decreases and the midlatitude pattern is strengthened  
315 consistent with equatorward wave propagation. Overall the wave pattern evolution is very

316 consistent with a downward wave coupling event: a stratospheric wave-1 anomaly at 10 hPa  
317 precedes a tropospheric wave-1 anomaly at 500 hPa and the wave-1 pattern exhibits an  
318 eastward phase tilt with height.

319 Downward wave coupling clearly impacts both the wave-1 amplitude and phase in the  
320 mid-troposphere. Since baroclinic scale wave numbers also contribute to the geopotential  
321 height at 500 hPa we consider the evolution of the full height anomaly field. Figure 6  
322 (top) shows the evolution of 500 hPa geopotential height anomaly averaged from 90°W to  
323 40°E as a function of latitude and time from  $-15$  to  $+15$  days during the downward wave  
324 coupling event together with the longitude-latitude patterns from 30°N to 90°N during the  
325 four stages (bottom). During the first stage the geopotential height anomaly involves a high  
326 wave number and is relatively weak. In the Atlantic sector there is only a small region of  
327 statistical significance near the pole. As the event evolves into the second stage a wave-1  
328 signal develops. The negative wave-1 anomaly is centered at 30°W with the positive lobe at  
329 150°E and coincides with the high-latitude wave-1 anomaly (see Fig. 5). As a result there is  
330 a large negative anomaly in the Atlantic region between 60 to 70°N. During the third stage  
331 the geopotential height anomaly exhibits a statistically significant wave-1 pattern poleward  
332 of 50°N and the phase of the pattern is identical to the wave-1 pattern shown in Fig. 5. In  
333 addition a positive anomaly develops in midlatitudes in the Atlantic region consistent with  
334 equatorward wave propagation. The positive anomaly clearly lags the negative anomaly from  
335 the second stage and in combination they resemble the positive phase of the North Atlantic  
336 Oscillation (NAO). The NAO is the leading mode of variability in the North Atlantic region,  
337 and represents a pressure see-saw between mid and high latitudes that reflects the position  
338 of the jet over the North Atlantic (Hurrell et al. 2003). Finally during the fourth stage the  
339 geopotential height anomalies in the Atlantic sector weaken significantly.

340 The NAO is associated with well-known weather regimes. In particular during the pos-  
341 itive phase there is a near-surface negative temperature anomaly over north-eastern North  
342 America and a positive anomaly over western Eurasia (Hurrell et al. 2003). Figure 7 (top)

343 shows the evolution of the 850 hPa temperature anomaly averaged from 60 to 80°N as a  
344 function of longitude and time from  $-15$  to  $+15$  days during the downward wave coupling  
345 event together with the longitude-latitude patterns from 30°N to 90°N during the four stages  
346 (bottom). Note that the near surface (2 meter) temperature evolution closely resembles the  
347 850 hPa temperature (not shown). During the first stage the anomalies are weak and there  
348 is only a small region of statistical significance near the pole. As the event proceeds through  
349 the second stage a negative anomaly appears over north-eastern North America and a posi-  
350 tive anomaly appears over northern Eurasia. The negative anomalies increase and peak at  
351 the beginning of the third stage and their location is consistent with the negative wave-1  
352 lobe over the Atlantic region. In contrast the positive anomalies reach a maximum at the  
353 end of the third stage. The evolution of the anomalies is consistent with advection of cold  
354 and warm air related to the anomalous flow associated with the wave-1 pattern over the  
355 Atlantic region. Finally during the fourth stage the wave-1 temperature pattern in the high  
356 latitude region weakens while the anomalies in midlatitudes remain large.

357 The evolution of the 850 hPa zonal wind anomaly averaged from 90°W to 40°E as a  
358 function of latitude and time from  $-15$  to  $+15$  days during the downward wave coupling  
359 event is shown in Fig. 8 (top). The longitude-latitude patterns from 30°N to 90°N during  
360 the four stages are also shown in Fig. 8 (bottom). As for the 850 hPa temperature anomaly,  
361 the largest impacts occur during the third stage when there is a clear wave-1 signature in  
362 high latitudes. In addition there is a clear poleward jet shift in the Atlantic region, which  
363 persists during stage four.

364 Finally, the evolution of mean sea level pressure anomaly averaged from 90°W to 40°E  
365 as a function of longitude and time from  $-15$  to  $+15$  days is shown in Fig. 9 (top). The  
366 longitude-latitude patterns from 30°N to 90°N during the four stages are also shown in Fig.  
367 9 (bottom). During the first stage the anomalies are weak and exhibit a high wave number  
368 similar to the 850 hPa temperature anomalies. During the second stage a negative mean  
369 sea level pressure anomaly develops in the Atlantic sector and reaches its minimum. The

370 negative anomaly is shifted slightly eastward relative to the geopotential height anomaly  
371 aloft. In addition the mean sea level pressure anomaly is consistent with the zonal index  
372 during this stage (see Fig. 3). A positive anomaly appears in midlatitudes during the third  
373 stage consistent with the positive NAO phase aloft. During the fourth stage the anomalies  
374 weaken significantly.

375 *c. Seasonal impact*

376 An individual downward wave coupling event has a statistically significant impact on  
377 the troposphere. The event occurs over a 28 day period with the impact in the troposphere  
378 focused during a 10 day period. While an individual event impacts the troposphere on a  
379 weekly timescale, several events may occur during an individual JFM season and thereby  
380 produce an impact on longer timescales. Here we consider the cumulative impacts in the  
381 troposphere during JFM seasons that are dominated by downward wave coupling between  
382 the stratosphere and the troposphere. In addition, we consider how the impacts differ from  
383 those during weak and strong vortex seasons, which have been studied extensively during  
384 recent years (e.g. Baldwin and Dunkerton 1999, 2001; Baldwin et al. 2003; Polvani and  
385 Waugh 2004).

386 The seasonal impact of wave-1 coupling is assessed using the wave-coupling index summed  
387 over JFM. Figure 10 shows the time series of the sum of the wave-coupling index during JFM  
388 from 1979 to 2011<sup>1</sup>. The stars (squares) indicate the eight years where the index exceeds  
389  $-0.25$  ( $+0.25$ ) standard deviations and represent years with large downward (upward) wave  
390 coupling. The 500 hPa wave-1 anomaly, the 500 hPa geopotential height anomaly, the  
391 850 hPa temperature anomaly and the mean sea level pressure anomaly during the years  
392 indicated by stars and squares are shown in Fig. 10 (middle and bottom, respectively).  
393 During years with a large negative wave-coupling index and hence large downward wave  
394 coupling the amplitude of the high-latitude total wave-1 pattern is large and dominated by

---

<sup>1</sup>Similar impacts are seen for December, January, February and March seasons.

395 the wave-1 anomaly (not shown). The high-latitude geopotential height anomaly at 500  
396 hPa is clearly dominated by the wave-1 anomaly. In addition, there is cooling over north-  
397 eastern North America and warming over north-western Eurasia. Finally the mean sea level  
398 pressure anomaly is negative in high latitudes in the Atlantic region with a positive anomaly  
399 in midlatitudes. All of these features are consistent with the positive phase of the NAO  
400 and were seen for the composite downward wave coupling event discussed in the previous  
401 subsection. Note that there are large signals in the North Pacific that were not seen in  
402 the individual event and likely reflect the potential impact of El-Nino/Southern Oscillation  
403 events, which do not average out because of the small sample size.

404 During years with a large positive wave-coupling index and hence large upward wave  
405 coupling the total and anomaly wave-1 pattern in high latitudes are very weak. The geopo-  
406 tential height anomaly in the Atlantic sector is weak and exhibits a pattern consistent with  
407 the negative phase of the NAO. The temperature anomaly involves warming over North  
408 America and cooling over Eurasia and the mean sea level pressure anomaly clearly reflects  
409 the geopotential height pattern at 500 hPa. Overall the response during years with a large  
410 positive wave-coupling index are opposite in sign to years with a large negative value, i.e.  
411 they are consistent with the negative phase of the NAO, however the anomalies for positive  
412 years are much weaker.

413 As discussed in the Introduction, a standard paradigm of the impact of the stratosphere  
414 on the troposphere is via weak/strong stratospheric polar vortex events, (e.g. Baldwin and  
415 Dunkerton 2001; Polvani and Waugh 2004). Therefore, we compare the seasonal composites  
416 of the wave-coupling index extremes with seasonal composites based on extremes of the zonal  
417 index. Figure 11 shows the time series of the average zonal-index at 30 hPa (the pc of the  
418 zonal-mean geopotential at 30 hPa) during JFM from 1979 to 2011<sup>2</sup>. The stars (squares)  
419 indicate the eight years where the average zonal index exceeds -0.25 (+0.25) standard de-

---

<sup>2</sup>Similar impacts occur for a zonal index defined at 10 hPa and for December, January, February and March seasons.

420 viations. Recall that the zonal index indicates the strength of the polar vortex. During  
421 years with a large negative zonal-index and hence a weak polar vortex there is a large high-  
422 latitude wave-1 anomaly that dominates the 500 hPa geopotential height anomaly. The 850  
423 hPa temperature anomaly involves warming over northern North America and cooling over  
424 Eurasia. The mean sea-level pressure anomaly is shifted eastward relative to the anomaly at  
425 500 hPa. Overall the patterns are consistent with the negative phase of the NAO. Note that  
426 only one of the eight weak vortex years corresponds with years with strong upward wave  
427 coupling (compare squares in Fig. 10 to stars in Fig. 11).

428 During years with a positive zonal-index and hence a strong polar vortex the high-latitude  
429 total and anomaly wave-1 pattern at 500 hPa are weaker and their sign and structure are  
430 reminiscent of the patterns seen during years with a large negative wave-coupling index (see  
431 Fig. 10). The high-latitude geopotential height at 500 hPa, the temperature at 850 hPa  
432 and the mean sea level pressure anomalies are all much weaker than during years with a  
433 weak vortex. The mean sea level pressure anomaly displays a significant zonal structure.  
434 Overall, the patterns are consistent with the positive phase of the NAO. Note that four out  
435 of the eight strong vortex years coincide with downward wave coupling years (compare stars  
436 in Fig. 10 to squares in Fig. 11). The tropospheric response during winter seasons with  
437 large downward wave coupling is larger than during years with a strong vortex (by a factor  
438 of 2). The composites suggest that the largest impact in the troposphere occurs during  
439 seasons with large downward wave coupling or a weak polar vortex, which correspond to the  
440 negative tails of the wave-coupling and zonal index histograms. The tropospheric impacts  
441 are associated with positive and negative phases of the NAO, respectively.

## 442 **4. Summary and discussion**

443 The life cycle of Northern Hemisphere downward wave coupling (wave reflection) between  
444 the stratosphere and troposphere has been analyzed using a composite approach. Downward

445 wave coupling events were isolated as extreme negative heat flux events using a daily wave-  
446 coupling index defined as the leading pc of the wave-1 heat flux at 30 hPa. The life cycle of  
447 the events spans a 28-day period.

448 The results illustrate that downward wave coupling from the stratosphere to the tropo-  
449 sphere involves large changes of the wave-1 pattern and basic state in the stratosphere. The  
450 event begins with a positive heat flux precursor in the stratosphere and a wave-1 pattern  
451 that exhibits a clear westward phase tilt from the mid-troposphere to the mid-stratosphere,  
452 indicating upward wave coupling. In addition, the polar vortex is conducive to upward wave  
453 propagation. A subsequent weakening of the polar vortex in the upper stratosphere pro-  
454 duces a region of negative vertical zonal-wind shear and therefore a region of vertical wave  
455 evanescence that acts as a vertical reflecting surface. The high-latitude wave-1 structure  
456 subsequently exhibits a clear eastward phase tilt from the mid troposphere to the upper  
457 stratosphere, indicating wave reflection and downward wave coupling. In addition, the total  
458 heat flux and vertical Eliassen-Palm flux are negative in the polar mid-to-lower stratosphere  
459 and the vertical flux divergence is positive. After the event, wave-1 exhibits a clear standing  
460 wave pattern and the polar vortex is strengthened.

461 Overall, the evolution in the stratosphere is very consistent with previous results by  
462 SPH10, Perlwitz and Harnik (2003), and Perlwitz and Harnik (2004) who investigated down-  
463 ward wave coupling on interseasonal and interannual timescales. In particular, the timescale  
464 of downward wave coupling events, the zonal-mean zonal-wind configuration and the wave-1  
465 pattern are all consistent with previous results. The life cycle of downward wave coupling  
466 events suggests that the upward propagating precursor plays an important role in the evolu-  
467 tion of the zonal-mean zonal wind and the formation the reflecting surface. The importance  
468 of the upward precursor was also highlighted by Harnik (2009) who showed that wave reflec-  
469 tion is associated with short timescale pulses of upward wave activity from the troposphere  
470 that produces a short timescale deceleration of the zonal-mean zonal wind and the subsequent  
471 reflection of the remaining wave activity. In addition the results suggest that downward wave

472 coupling events modify the wave-driven residual (Brewer-Dobson) circulation via changes in  
473 wave-1 heat flux in the stratosphere. The detailed impact of the events on the circulation  
474 will be reported elsewhere.

475 The current study quantifies for the first time the impact of downward wave coupling  
476 on the troposphere. The impact in the troposphere is associated with a transition over a  
477 10-day period toward a positive phase of the NAO and follows the wave reflection event in  
478 the stratosphere. The NAO signal develops as a result of a large amplitude high-latitude  
479 wave-1 anomaly at 500 hPa that exhibits a clear westward phase progression and is directly  
480 coupled to the wave-1 evolution at 10 hPa. The negative lobe of the high-latitude wave-1  
481 anomaly at 500 hPa is followed by a positive anomaly in midlatitudes due to equatorward  
482 propagation that together produce a positive NAO pattern. The impacts on near surface  
483 circulation and temperature during the event are consistent with those observed during the  
484 positive phase of the NAO. The adjustment of the polar vortex to the negative heat flux  
485 forcing also contributes to the mean sea level pressure anomaly.

486 The impacts in the troposphere are in agreement with previous statistical results by  
487 Perlwitz and Graf (1995) who highlighted a non-zonal connection between the stratosphere  
488 and the tropospheric geopotential height that is most pronounced in the Atlantic region.  
489 The mean sea level pressure anomalies associated with the vortex adjustment process is  
490 consistent with the results of Black (2002) and Ambaum and Hoskins (2002). Ambaum  
491 and Hoskins (2002) suggested that a positive NAO phase typically occurs as a result of a  
492 strengthened polar vortex that is associated with equatorward propagation of wave-activity  
493 in the stratosphere. However, the present study reveals that a positive NAO pattern is  
494 generated as a result of wave-1 reflection in the stratosphere, the subsequent growth of  
495 a high-latitude wave-1 pattern in the troposphere and a midlatitude anomaly that arises  
496 from equatorward propagation. The westward phase progression of the high-latitude wave-1  
497 pattern during the events suggests that the stratosphere can impact tropospheric weather  
498 through non-stationary planetary scale waves. The role of quasi-stationary waves in forcing

499 zonal wind anomalies in the troposphere during northern winter is consistent with DeWeaver  
500 and Nigam (2000). However, a detailed understanding of how wave reflection events impact  
501 the subtropical jet requires further research.

502 Winter seasons with multiple downward wave coupling events, as indicated by a large  
503 cumulative negative wave-coupling index, exhibit pronounced impacts on tropospheric cli-  
504 mate that are consistent with those seen during the composite life cycle. In particular, the  
505 overall geopotential height, near surface temperature and mean sea level pressure anomalies  
506 are characteristic of the positive phase of the NAO. During years with large upward wave  
507 coupling, as indicated by a large cumulative positive index, the impacts are consistent with  
508 the negative phase of the NAO, however the magnitude of the anomalies is much weaker  
509 than during years with a large downward wave coupling. This result suggests that upward  
510 wave propagation is not a process that directly leads to large impacts on the tropospheric  
511 circulation.

512 The seasonal impact of large wave-1 heat flux events were compared to JFM seasons  
513 with a weak and strong vortex as measured by the average zonal index in the stratosphere.  
514 The present analysis confirms previous studies (e.g. Baldwin and Dunkerton 2001; Polvani  
515 and Waugh 2004) that seasons with an extreme negative (positive) zonal index and hence  
516 a weak (strong) stratospheric polar vortex exhibit tropospheric anomalies consistent with  
517 the negative (positive) phase of the NAO with the magnitude of tropospheric anomalies  
518 being larger for weak vortex events. However, the present analysis also reveals that the  
519 tropospheric anomalies during years with an extreme positive zonal index are considerably  
520 weaker than during years with extreme negative wave-coupling index suggesting that wave  
521 reflection has a larger impact on the tropospheric circulation than the poleward refraction  
522 of planetary waves in the stratosphere. While the results suggest important links between  
523 the stratospheric seasonal indices and the phase of the NAO, further analysis with longer  
524 data sets is required to establish the statistical significance of the seasonal impacts.

525 The close link between the stratosphere and the NAO phase has been documented by

526 many previous authors (e.g. Perlwitz and Graf 1995; Thompson and Wallace 1998; Kuroda  
527 and Kodera 1999). This link is conventionally associated with different phases of a single  
528 index, e.g. weak and strong vortex events (Baldwin and Dunkerton 1999, 2001). The current  
529 results suggest that the connection between the stratosphere and the NAO, including the  
530 impacts on tropospheric weather and climate, involves two distinct dynamical mechanisms  
531 that are best described by the negative tails of the wave-coupling and zonal indices, e.g.  
532 stratospheric wave reflection and sudden stratospheric warmings due to wave absorption,  
533 respectively. The positive tails of the two indices have a much weaker impact on the tro-  
534 posphere suggesting that the relationship between these two indices is not linear, namely  
535 strong (weak) vortex events are not equivalent to downward (upward) wave coupling events.  
536 A detailed understanding of the relationship between the wave-coupling and zonal indices  
537 during the different events is the subject of future investigation.

538 The impact of downward wave coupling events on tropospheric weather and climate has  
539 not been previously recognized because long-timescale and latitudinal averages are typically  
540 applied when calculating the vortex events and their relation to heat flux events (Newman  
541 et al. 2001; Polvani and Waugh 2004; Limpasuvan et al. 2004). Our life cycle analysis  
542 shows that the impacts in the troposphere occur on weekly timescales consistent with wave  
543 propagation and predominately for wave-1. In addition the pc index times series encodes the  
544 latitudinal structure of the leading mode of heat flux variability and thus does not require  
545 any latitudinal averaging that may mask a large positive/negative meridional dipole pattern.  
546 Hurwitz et al. (2011) suggested that the recent strong (and cold) vortex winter seasons in  
547 1997 and 2011 are due to weak upward heat flux from the troposphere. An investigation of the  
548 role of wave reflection during these winters may provide additional insight. Several previous  
549 authors have discussed the role of wave interference in stratosphere-troposphere coupling  
550 (Garfinkel et al. 2011; Smith et al. 2010; Fletcher and Kushner 2011; Smith et al. 2011;  
551 Smith and Kushner 2012). Although linear interference is likely an important mechanism in  
552 the upper stratosphere where the wave-1 heat flux variability occurs in the vicinity of the

553 climatology, in the lower stratosphere and troposphere the impacts of wave reflection are  
554 focused in high latitudes where the climatological pattern is weak.

555 Overall, the results suggest that stratosphere-troposphere coupling events should be de-  
556 fined using both wave-coupling and zonal-mean indices and the impacts in the troposphere  
557 should be considered on weather and climate timescales (weekly to interannual). The im-  
558 plications of the connection between downward wave coupling and the NAO phase suggests  
559 that general circulation models that do not include a proper representation of stratosphere-  
560 troposphere dynamical coupling associated with wave reflection, e.g. Shaw and Perlwitz  
561 (2010), may be missing an amplifying factor of the NAO evolution, which is important for  
562 capturing trends in the NAO phase, e.g. Scaife et al. (2005).

563 *Acknowledgments.*

564 TAS is supported by the National Science Foundation under grant AGS-1129519. JP ac-  
565 knowledges support by NOAA's Climate Program Office. We thank the ECMWF for provid-  
566 ing the ERA-Interim reanalysis data set, Dr. Nili Harnik for the use of her quasi-geostrophic  
567 model and for helpful comments, Dr. Mark Baldwin for his EOF code, and finally to Drs.  
568 Limpasuvan and McDaniel for their help with the statistical significance calculations. The  
569 authors are grateful to three anonymous reviewers and Dr. Dave Thompson whose comments  
570 helped improve the manuscript.

## REFERENCES

- 573 Ambaum, M. H. P. and B. J. Hoskins, 2002: The NAO troposphere-stratosphere connection.  
574 *J. Climate*, **15**, 1969–1978.
- 575 Baldwin, M. P. and T. J. Dunkerton, 1999: Downward propagation of the arctic oscillation  
576 from the stratosphere to the troposphere. *J. Geophys. Res.*, **104**, 30 937–30 946.
- 577 Baldwin, M. P. and T. J. Dunkerton, 2001: Stratospheric harbingers of anomalous weather  
578 regimes. *Science*, **294**, 581–584.
- 579 Baldwin, M. P., D. B. Stephenson, and I. T. Jolliffe, 2009: Spatial weighting and iterative  
580 projection methods for EOFs. *J. Climate*, **22**, 234–243.
- 581 Baldwin, M. P., D. B. Stevenson, D. W. J. Thompson, T. J. Dunkerton, A. J. Charlton,  
582 and A. O'Neill, 2003: Stratospheric memory and skill of extended-range weather forecasts.  
583 *Science*, **301**, 636–640.
- 584 Black, R. X., 2002: Stratospheric forcing of surface climate in the Arctic Oscillation. *J.*  
585 *Climate*, **15**, 268–277.
- 586 Christiansen, B., 2001: Downward propagation of zonal mean zonal wind anomalies from  
587 the stratosphere to the troposphere: Model and reanalysis. *J. Geophys. Res.*, **104**, 30 937–  
588 30 946.
- 589 Dee, D. P., et al., 2011: The ERA-Interim reanalysis: configuration and performance of the  
590 data assimilation system. *Quart. J. R. Meteor. Soc.*, **137**, 553–597.
- 591 DeWeaver, E. and S. Nigam, 2000: Do stationary waves drive the zonal-mean jet anomalies  
592 of the northern winter? *J. Climate*, **13**, 2160–2176.

593 Fletcher, C. G. and P. J. Kushner, 2011: The role of linear interference in the annular mode  
594 response to tropical SST forcing. *J. Climate*, **24**, 778–794.

595 Garfinkel, C. I., D. L. Hartmann, and F. Sassi, 2011: Tropospheric precursors  
596 of anomalous northern hemisphere stratospheric polar vortices. *J. Climate*, **23**,  
597 10.1175/2010JCLI3010.1.

598 Gerber, E. P., et al., 2012: Assessing and understanding the impact of stratospheric  
599 dynamics and variability on the earth system. *Bull. Amer. Met. Soc.*, 845–859, doi:  
600 10.1175/BAMS-d-11-00145.1.

601 Harnik, N., 2009: Observed stratospheric downward reflection and its relation to upward  
602 pulses of wave activity. *J. Geophys. Res*, **114**, doi:10.1029/2008JD010493.

603 Harnik, N. and R. S. Lindzen, 2001: The effect of reflecting surfaces on the vertical structure  
604 and variability of stratospheric planetary waves. *J. Atmos. Sci.*, **58**, 2872–2894.

605 Hartley, D. E., J. T. Vilarin, R. X. Black, and C. A. Davis, 1998: A new perspective on the  
606 dynamical link between the stratosphere and troposphere. *Nature*, **391**, 471–474.

607 Hartmann, D. L., J. M. Wallace, V. Limpasuvan, D. W. J. Thompson, and J. R. Holton,  
608 2000: Can ozone depletion and global warming interact to produce rapid climate change?  
609 *Proc. Natl. Acad. Sci.*, **97**, 1412–1417.

610 Haynes, P. H., 2005: Stratospheric dynamics. *Annu. Rev. Fluid Mech.*, **37**, 263–293.

611 Hurrell, J. W., Y. Kushnir, M. Visbeck, and G. Ottersen, 2003: An overview of the north  
612 atlantic oscillation. The north atlantic oscillation: Climate significance and environmental  
613 impact. *Geophysical Monograph Series*, **134**, 1–35.

614 Hurwitz, M. M., P. A. Newman, and C. I. Garfinkel, 2011: The Arctic vortex in march 2011:  
615 A dynamical perspective. *Atmos. Chem. Phys.*, **11**, 11 447–11 453.

616 Kuroda, Y. and K. Kodera, 1999: Role of planetary waves in the stratosphere-troposphere  
617 coupled variability in the northern hemisphere winter. *Geophys. Res. Lett.*, **26**, 23752378.

618 Limpasuvan, V., D. J. Thompson, and D. L. Hartmann, 2004: The life cycle of the northern  
619 hemisphere sudden stratospheric warmings. *J. Climate*, **17**, 2584–2596.

620 Newman, P. A., E. R. Nash, and J. E. Rosenfield, 2001: What controls the temperature in  
621 the Arctic stratosphere in the spring? *J. Geophys. Res.*, **106**, 19999–20010.

622 North, G. R., T. L. Bell, R. F. Cahalan, and F. J. Moeng, 1982: Sampling errors in the  
623 estimation of empirical orthogonal functions. *Mon. Wea. Rev.*, **110**, 699–706.

624 Perlwitz, J. and H.-F. Graf, 1995: The statistical connection between tropospheric and  
625 stratospheric circulation of the northern hemisphere in winter. *J. Climate*, **8**, 2281–2295.

626 Perlwitz, J. and N. Harnik, 2003: Observational evidence of a stratospheric influence on the  
627 troposphere by planetary wave reflection. *J. Climate*, **16**, 3011–3026.

628 Perlwitz, J. and N. Harnik, 2004: Downward coupling between the stratosphere and tropo-  
629 sphere: The relative roles of wave and zonal mean processes. *J. Climate*, **17**, 4902–4909.

630 Plumb, R. A. and K. Semeniuk, 2003: Downward migration of extratropical zonal wind  
631 anomalies. *J. Geophys. Res.*, **108**, doi:10.1029/2002JD002773.

632 Polvani, L. M. and P. J. Kushner, 2002: Tropospheric response to stratospheric perturbations  
633 in a relatively simple general circulation model. *Geophys. Res. Lett.*, **29**, doi:10.1029/  
634 2001GL014284.

635 Polvani, L. M. and D. Waugh, 2004: Upward wave activity flux as a precursor to extreme  
636 stratospheric events and subsequent anomalous surface weather regimes. *J. Climate*, **17**,  
637 3548–3554.

638 Randel, W. J., 1987: A study of planetary waves in the southern winter troposphere and  
639 stratosphere. Part I: Wave structure and vertical propagation. *J. Atmos. Sci.*, **44**, 917–935.

640 Scaife, A. A., J. R. Knight, G. K. Vallis, and C. K. Folland, 2005: A stratospheric influence  
641 on the winter NAO and north atlantic surface climate. *Geophys. Res. Lett.*, **32**, doi:10.  
642 1029/2005GL023226.

643 Shaw, T. A. and J. Perlwitz, 2010: The impact of stratospheric model configuration on  
644 planetary-scale waves in northern hemisphere winter. *J. Climate*, **23**, 3369–3389.

645 Shaw, T. A., J. Perlwitz, and N. Harnik, 2010: Downward wave coupling between the  
646 stratosphere and troposphere: The importance of meridional wave guiding and comparison  
647 with zonal-mean coupling. *J. Climate*, **23**, 6365–6381.

648 Shaw, T. A. and T. G. Shepherd, 2008: Raising the roof. *Nature Geosc.*, **1**, 12–13.

649 Smith, K. L., C. G. Fletcher, and P. J. Kushner, 2010: The role of linear interference in the  
650 annular mode response to extratropical surface forcings. *J. Climate*, **23**, 6036–6050.

651 Smith, K. L. and P. J. Kushner, 2012: Linear interference in extratropical stratosphere-  
652 troposphere interactions. *J. Geophys. Res.*, in press.

653 Smith, K. L., P. J. Kushner, and J. Cohen, 2011: The role of linear interference in northern  
654 annular mode variability associated with Eurasian snow cover extent. *J. Climate*, **24**,  
655 6185–6202.

656 Song, W. and W. A. Robinson, 2004: Dynamical mechanisms for stratospheric influences on  
657 the troposphere. *J. Atmos. Sci.*, **61**, 1711–1725.

658 Thompson, D. W. J. and J. M. Wallace, 1998: The Arctic Oscillation signature in the  
659 wintertime geopotential height and temperature fields. *Geophys. Res. Lett.*, **25**, 1297–  
660 1300.

661 **List of Tables**

662 1 Central date of downward wave coupling events at 30 hPa and the minimum  
663 total wave-1 heat flux from 40 to 90°N during the event 28

TABLE 1. Central date of downward wave coupling events at 30 hPa and the minimum total wave-1 heat flux from 40 to 90°N during the event

Date	$\min_{40-90^\circ\text{N}} v'T'$ (Kms <sup>-1</sup> )
02/24/1979	-99.37
01/18/1984	-38.30
01/22/1986	-47.30
02/22/1989	-75.81
02/11/1990	-77.66
01/28/1991	-80.75
01/21/1992	-31.94
03/15/1993	-41.18
02/11/1995	-78.63
01/09/1996	-64.24
01/21/1997	-31.71
01/31/2005	-29.27
01/08/2007	-41.99
01/26/2008	-76.00

## 664 List of Figures

- 665 1 Top: The climatological zonal-mean wave-1 heat flux during January, Febru-  
666 ary and March (left), the wave-1 heat flux pattern found by regressing the  
667 heat flux at all levels on the standardized 30 hPa pc time series (middle) and  
668 the total wave-1 heat flux field for a  $\sigma_{JFM} = -1.7$  value of the standardized  
669 principle component, e.g. the climatological heat flux pattern is added to  
670  $\sigma_{JFM}$  times the regression pattern (right). Contour interval is logarithmic in  
671 powers of 2, e.g.  $\pm[1, 2, 4, 8, 16, 32, 64, 128, 256]$   $\text{Kms}^{-1}$ , negative contours  
672 are dashed and the thick solid line indicates the zero contour. Bottom: The  
673 histogram of the daily JFM values of the leading pc at 30 hPa. 32
- 674 2 Top: The evolution of the wave-1 heat flux anomaly projected onto the re-  
675 gression pattern in Fig. 1 (top, middle) for the composite downward wave  
676 coupling event as a function of time from  $-15$  to  $15$  days and height. Contour  
677 interval is  $0.25$ , negative contours are dashed and the thick solid line indicates  
678 the zero contour. Anomalous zonal-mean wave-1 meridional heat flux (mid-  
679 dle) and negative meridional momentum flux (bottom) averaged from  $-12$  to  
680  $-6$ ,  $-5$  to  $1$ ,  $2$  to  $8$  and  $9$  to  $15$  days. Contour interval as in Fig. 1 for middle  
681 panel and equal to  $\pm[1, 2, 4, 8, 16, 32, 64, 128, 256]$   $\text{m}^2\text{s}^{-2}$  for bottom panel.  
682 Shading indicates statistical significance at the 95% level based on a t-test. 33
- 683 3 Top: The evolution of the zonal index (e.g. the leading pc of the zonal-  
684 mean geopotential height at each pressure level) for the composite downward  
685 wave coupling event as a function of time from  $-15$  to  $15$  days and height.  
686 Contouring as in Fig. 2 (top). Bottom: Anomalous zonal-mean zonal wind  
687 averaged from  $-12$  to  $-6$ ,  $-5$  to  $1$ ,  $2$  to  $8$  and  $9$  to  $15$  days. Contour interval  
688 is  $1 \text{ ms}^{-1}$ . Shading indicates statistical significance at the 95% level based on  
689 a t-test. 34

- 690 4 The evolution (from top to bottom) of the total zonal-mean zonal wind, total  
691 wave-1 meridional heat flux, total negative wave-1 meridional momentum flux  
692 and total wave-1 geopotential height at  $70^{\circ}\text{N}$  for the composite downward wave  
693 coupling event averaged from  $-12$  to  $-6$ ,  $-5$  to  $1$ ,  $2$  to  $8$  and  $9$  to  $15$  days.  
694 Shading in top panel indicates regions of wave evanescence. Contour interval  
695 is  $5 \text{ ms}^{-1}$  (first row), logarithmic in powers of 2, e.g.  $\pm[1, 2, 4, 8, 16, 32, 64,$   
696  $128, 256]$   $\text{Kms}^{-1}$  (second row) and  $\text{m}^2\text{s}^{-2}$  (third row) and  $\pm 1.e2[1, 2, 4, 8, 16,$   
697  $32, 64, 128, 256]$  m (fourth row). Negative contours are dashed and the thick  
698 solid line indicates the zero contour. 35
- 699 5 Top: The evolution of the total 500 hPa (black contours) and 10 hPa (color  
700 contours) wave-1 averaged from  $60$  to  $80^{\circ}\text{N}$  for the composite downward wave  
701 coupling event as a function of time from  $-20$  to  $20$  days and longitude.  
702 Contour interval is  $20$  m (color contours) and  $10$  m (black contours). Bottom:  
703 The total 500 hPa wave-1 averaged from  $-12$  to  $-6$ ,  $-5$  to  $1$ ,  $2$  to  $8$  and  $9$  to  
704  $15$  days. Contour interval is  $10$  m. 36
- 705 6 Top: The evolution of the 500 hPa geopotential height anomaly averaged from  
706  $90^{\circ}\text{W}$  to  $40^{\circ}\text{E}$  for the composite downward wave coupling event as a function  
707 of time from  $-20$  to  $20$  days and latitude. Bottom: The 500 hPa geopotential  
708 height anomaly averaged from  $-12$  to  $-6$ ,  $-5$  to  $1$ ,  $2$  to  $8$  and  $9$  to  $15$  days.  
709 Contour interval is  $10$  m. Shading indicates statistical significance at the 95%  
710 level based on a t-test. 37
- 711 7 Top: The evolution of the 850 hPa temperature anomaly averaged from  $60$   
712 to  $80^{\circ}\text{N}$  for the composite downward wave coupling event as a function of  
713 time from  $-20$  to  $20$  days and longitude. Bottom: The anomalous 850 hPa  
714 temperature averaged from  $-12$  to  $-6$ ,  $-5$  to  $1$ ,  $2$  to  $8$  and  $9$  to  $15$  days.  
715 Contour interval is  $0.5$  K. Shading indicates statistical significance at the 95%  
716 level based on a t-test. 38

- 717 8 Top: The evolution of the 850 hPa zonal wind anomaly averaged from 90°W  
718 to 40°E for the composite downward wave coupling event as a function of time  
719 from -20 to 20 days and latitude. Bottom: The anomalous 850 hPa zonal  
720 wind averaged from -12 to -6, -5 to 1, 2 to 8 and 9 to 15 days. Contour  
721 interval is 0.5 ms<sup>-1</sup>. Shading indicates statistical significance at the 95% level  
722 based on a t-test. 39
- 723 9 Top: The evolution of the mean sea level pressure anomaly averaged from  
724 90°W to 40°E for the composite downward wave coupling event as a function  
725 of time from -20 to 20 days and latitude. Bottom: The anomalous mean sea  
726 level pressure averaged from -12 to -6, -5 to 1, 2 to 8 and 9 to 15 days.  
727 Contour interval is 1 hPa. Shading indicates statistical significance at the  
728 95% level based on a t-test. 40
- 729 10 Top: Sum of the JFM wave-coupling index (leading pc of the wave-1 flux at  
730 30 hPa) as a function of year. Middle: The 500 hPa wave-1, the 500 hPa  
731 geopotential height, the 850 hPa temperature and the mean sea level pressure  
732 anomalies during years with a star. Bottom: Same as middle but for years  
733 with a square. Contour interval is 5 m for 500 hPa wave-1 and 500 hPa  
734 geopotential height anomalies, 0.25 K for 850 hPa temperature anomaly and  
735 0.5 hPa for mean sea level pressure anomaly. 41
- 736 11 Top: The JFM average zonal-index (leading pc of the zonal-mean geopotential  
737 at 30 hPa) as a function of year. Middle: The 500 hPa wave-1, the 500 hPa  
738 geopotential height, the 850 hPa temperature and the mean sea level pressure  
739 anomalies during years with a star. Bottom: Same as middle but for years  
740 with a square. Contouring as in Fig. 10. 42

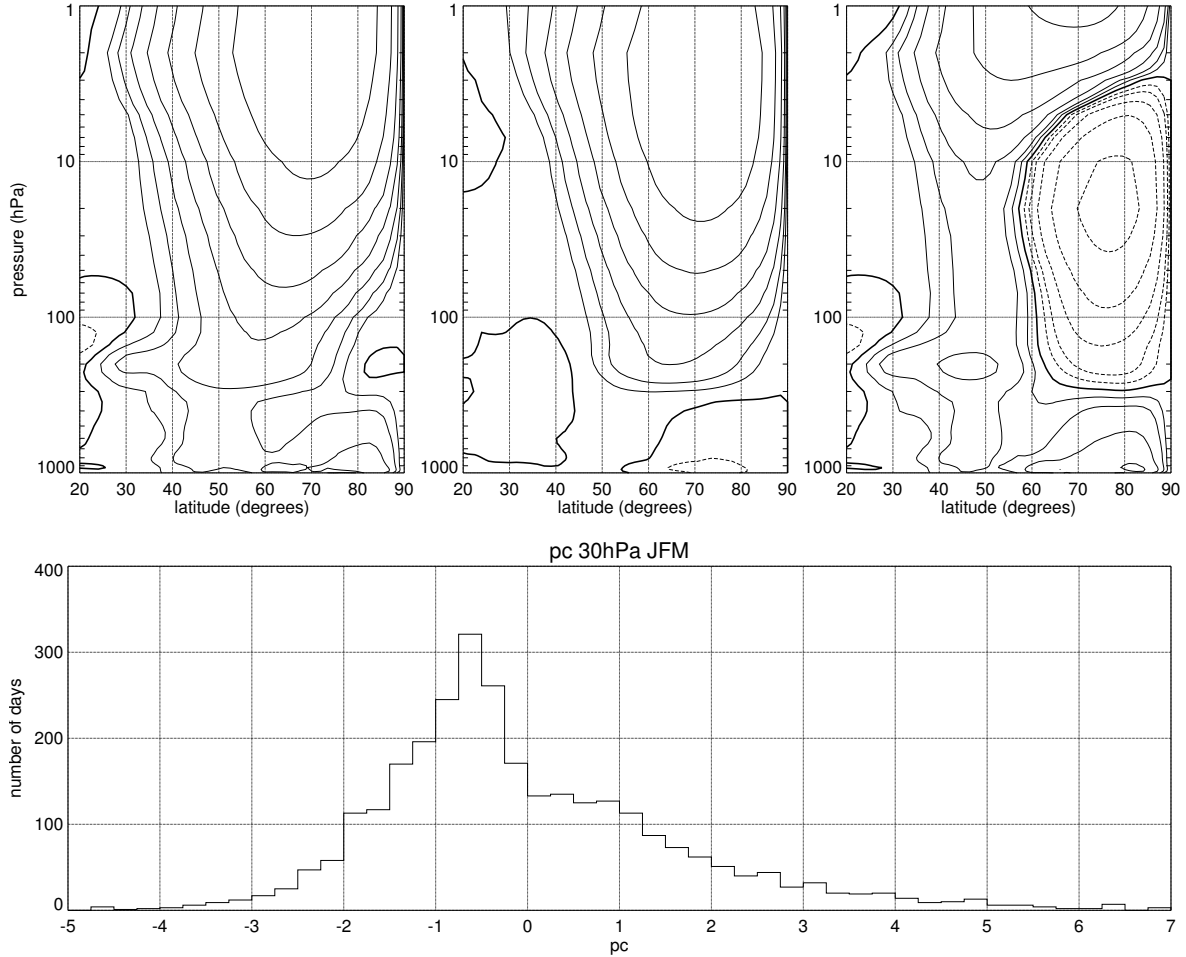


FIG. 1. Top: The climatological zonal-mean wave-1 heat flux during January, February and March (left), the wave-1 heat flux pattern found by regressing the heat flux at all levels on the standardized 30 hPa pc time series (middle) and the total wave-1 heat flux field for a  $\sigma_{JFM} = -1.7$  value of the standardized principle component, e.g. the climatological heat flux pattern is added to  $\sigma_{JFM}$  times the regression pattern (right). Contour interval is logarithmic in powers of 2, e.g.  $\pm[1, 2, 4, 8, 16, 32, 64, 128, 256]$   $\text{Kms}^{-1}$ , negative contours are dashed and the thick solid line indicates the zero contour. Bottom: The histogram of the daily JFM values of the leading pc at 30 hPa.

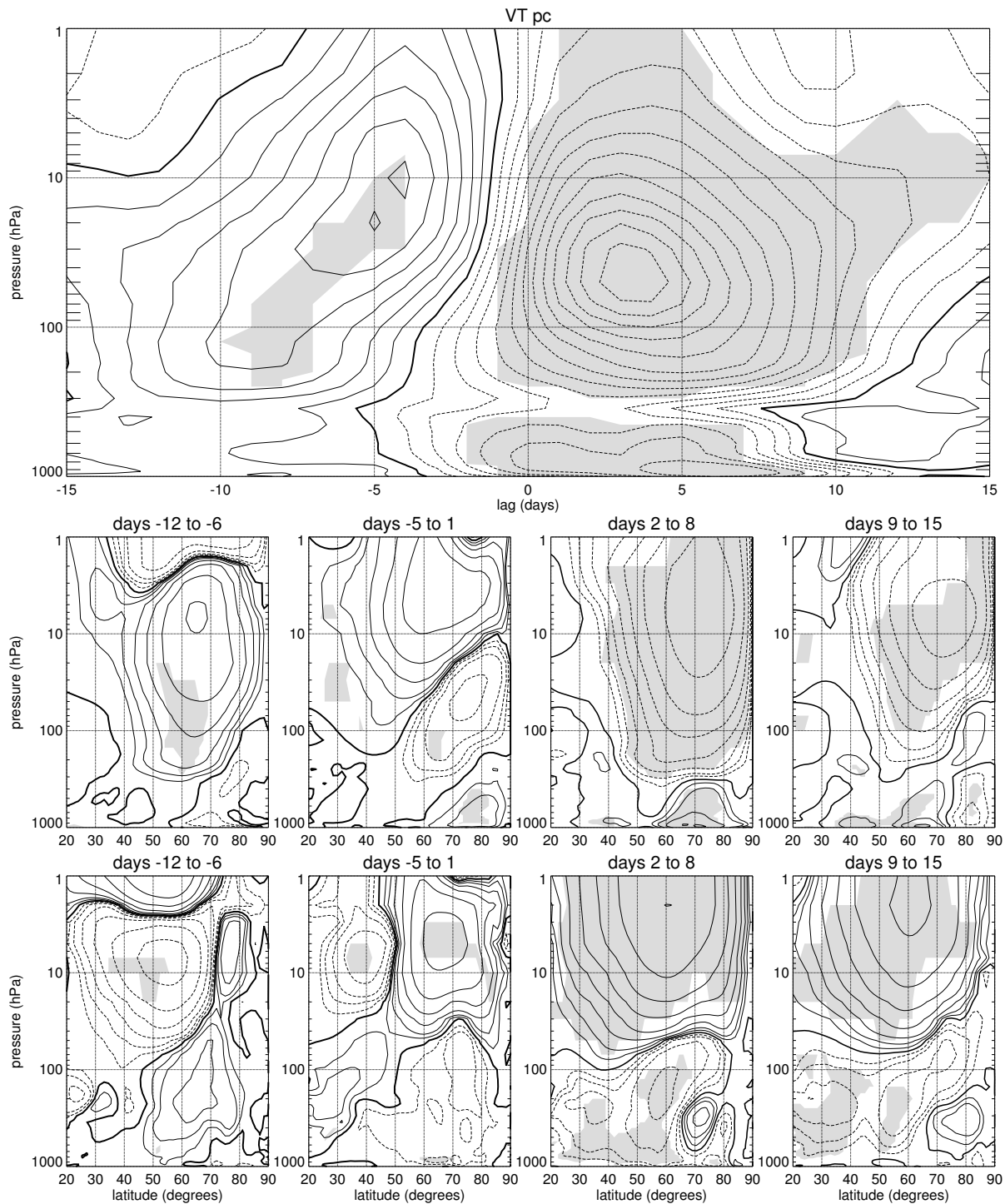


FIG. 2. Top: The evolution of the wave-1 heat flux anomaly projected onto the regression pattern in Fig. 1 (top, middle) for the composite downward wave coupling event as a function of time from  $-15$  to  $15$  days and height. Contour interval is  $0.25$ , negative contours are dashed and the thick solid line indicates the zero contour. Anomalous zonal-mean wave-1 meridional heat flux (middle) and negative meridional momentum flux (bottom) averaged from  $-12$  to  $-6$ ,  $-5$  to  $1$ ,  $2$  to  $8$  and  $9$  to  $15$  days. Contour interval as in Fig. 1 for middle panel and equal to  $\pm[1, 2, 4, 8, 16, 32, 64, 128, 256]$   $\text{m}^2\text{s}^{-2}$  for bottom panel. Shading indicates statistical significance at the 95% level based on a  $t$ -test.

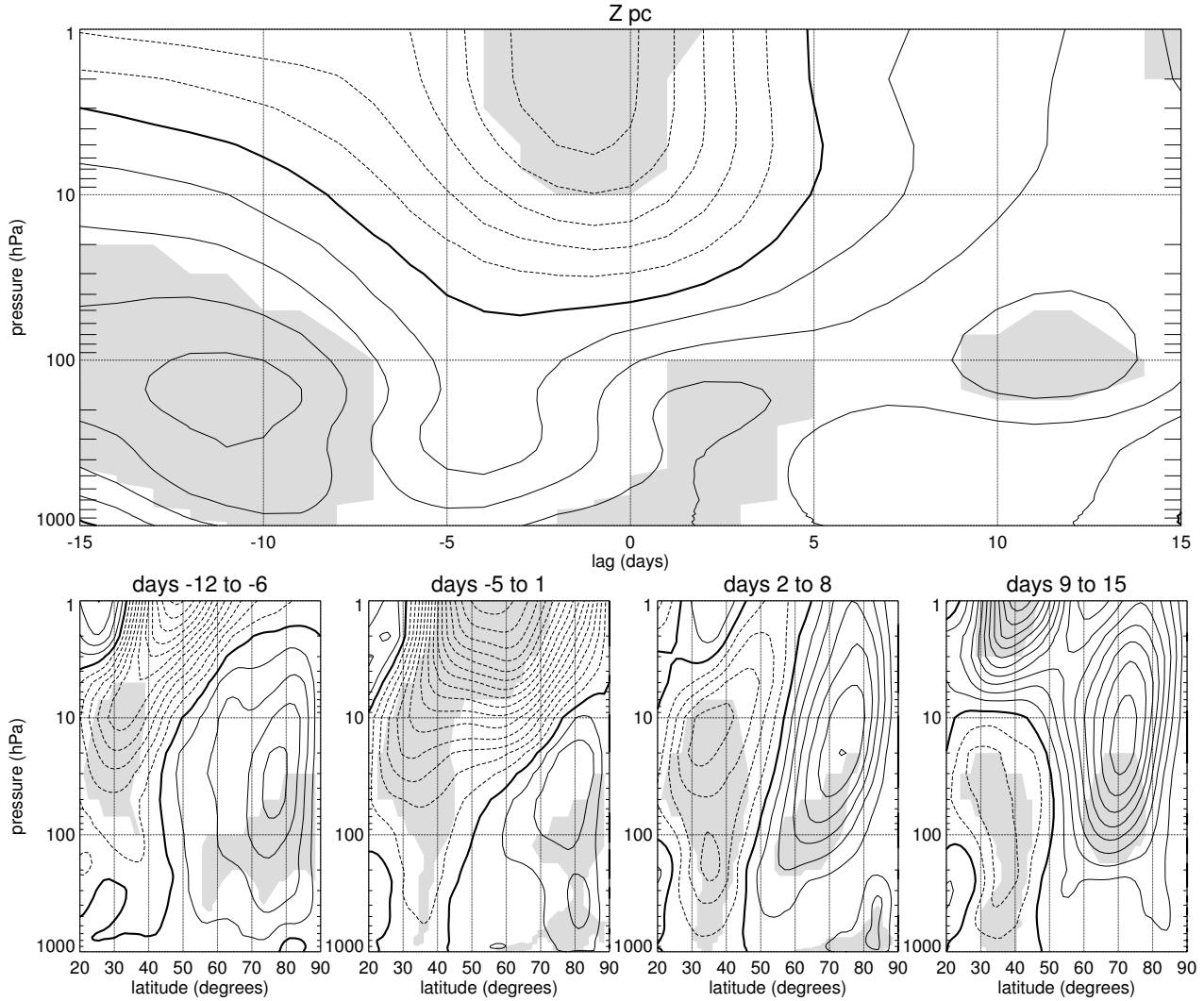


FIG. 3. Top: The evolution of the zonal index (e.g. the leading pc of the zonal-mean geopotential height at each pressure level) for the composite downward wave coupling event as a function of time from  $-15$  to  $15$  days and height. Contouring as in Fig. 2 (top). Bottom: Anomalous zonal-mean zonal wind averaged from  $-12$  to  $-6$ ,  $-5$  to  $1$ ,  $2$  to  $8$  and  $9$  to  $15$  days. Contour interval is  $1 \text{ ms}^{-1}$ . Shading indicates statistical significance at the 95% level based on a t-test.

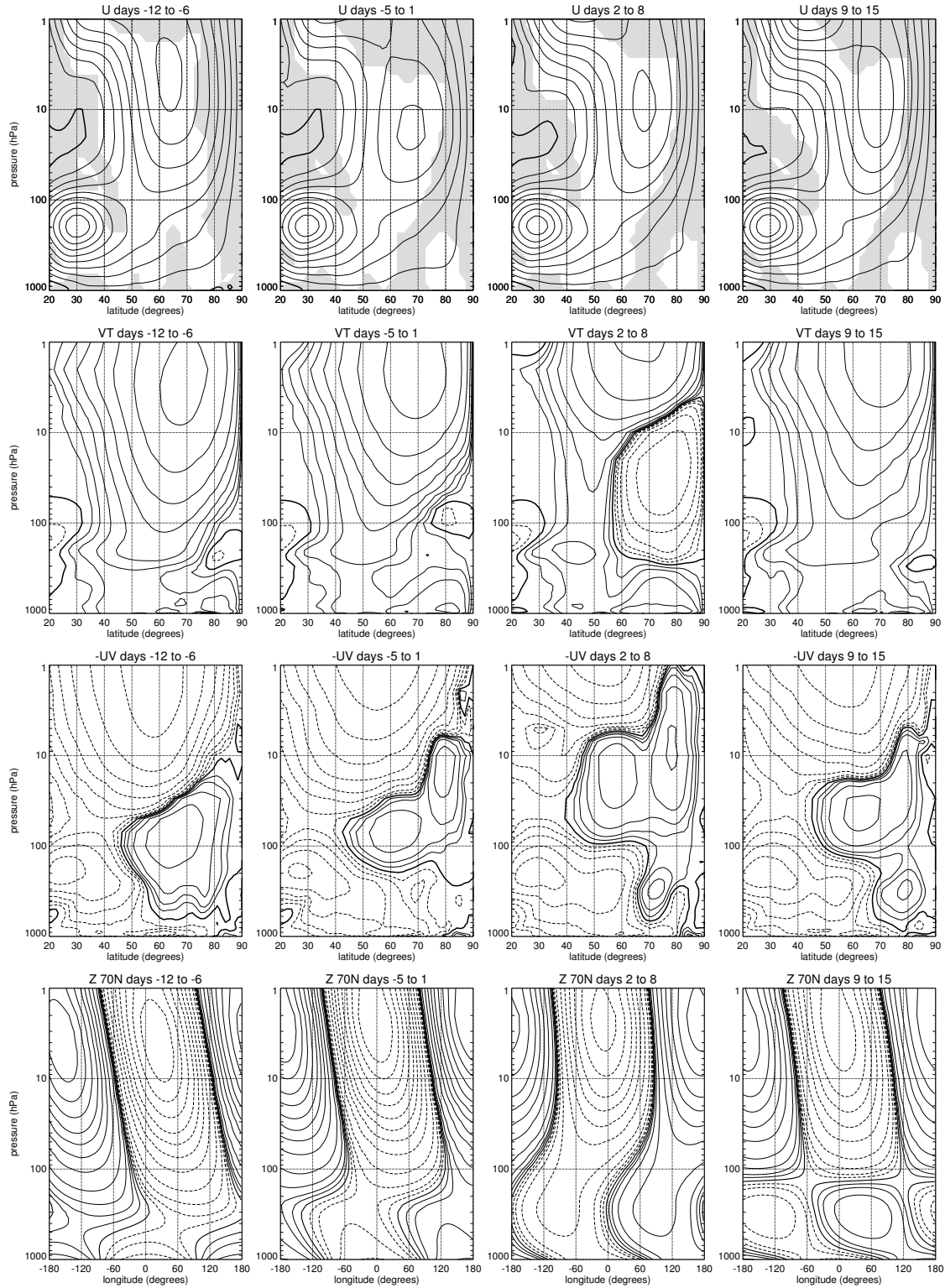


FIG. 4. The evolution (from top to bottom) of the total zonal-mean zonal wind, total wave-1 meridional heat flux, total negative wave-1 meridional momentum flux and total wave-1 geopotential height at  $70^\circ\text{N}$  for the composite downward wave coupling event averaged from  $-12$  to  $-6$ ,  $-5$  to  $1$ ,  $2$  to  $8$  and  $9$  to  $15$  days. Shading in top panel indicates regions of wave evanescence. Contour interval is  $5 \text{ ms}^{-1}$  (first row), logarithmic in powers of 2, e.g.  $\pm[1, 2, 4, 8, 16, 32, 64, 128, 256] \text{ Kms}^{-1}$  (second row), and  $\pm 1.e2[1, 2, 4, 8, 16, 32, 64, 128, 256] \text{ m}^2\text{s}^{-2}$  (third row) and  $\pm 1.e2[1, 2, 4, 8, 16, 32, 64, 128, 256] \text{ m}$  (fourth row). Negative contours are dashed and the thick solid line indicates the zero contour.

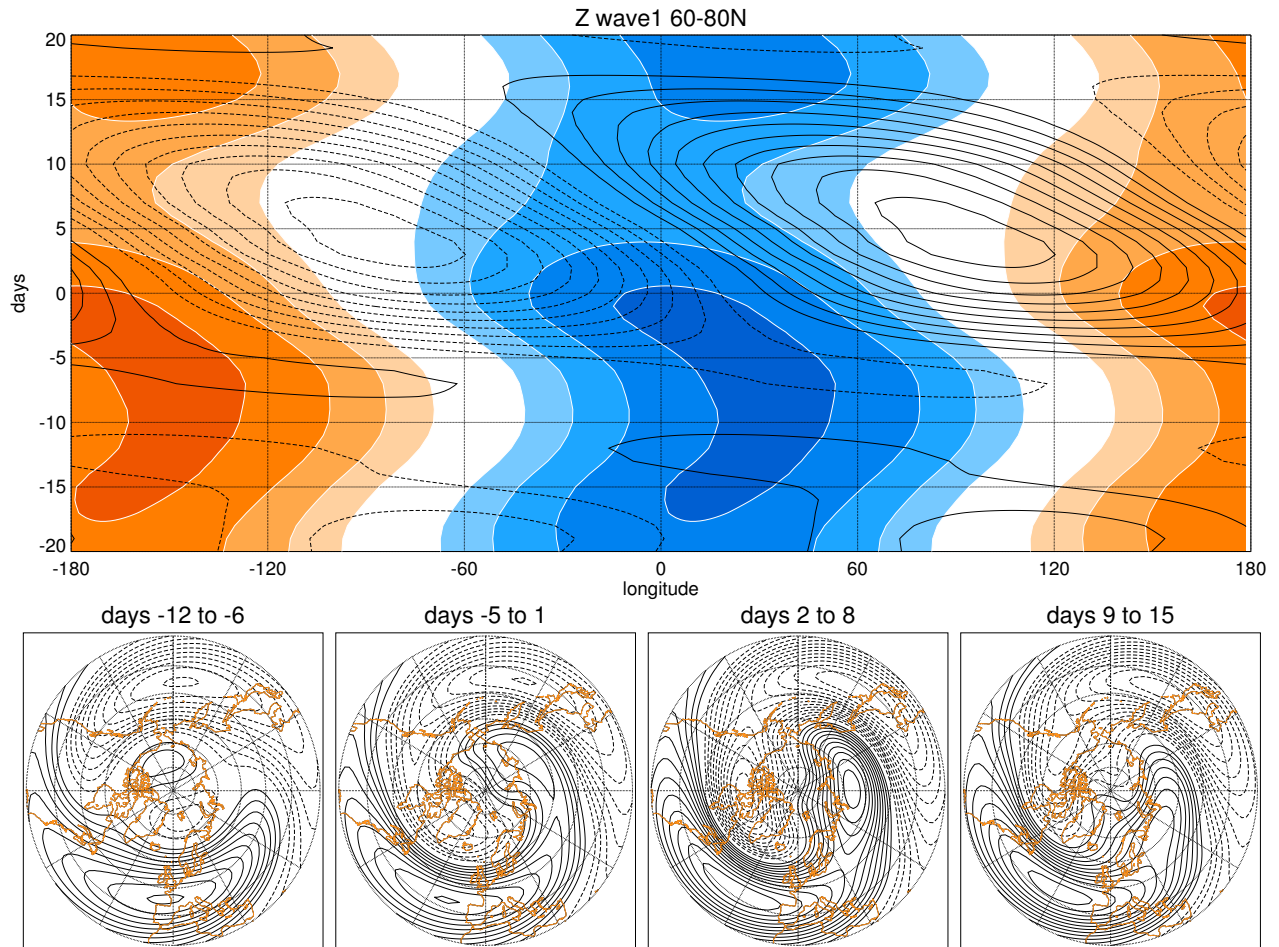


FIG. 5. Top: The evolution of the total 500 hPa (black contours) and 10 hPa (color contours) wave-1 averaged from 60 to 80°N for the composite downward wave coupling event as a function of time from  $-20$  to  $20$  days and longitude. Contour interval is 20 m (color contours) and 10 m (black contours). Bottom: The total 500 hPa wave-1 averaged from  $-12$  to  $-6$ ,  $-5$  to  $1$ ,  $2$  to  $8$  and  $9$  to  $15$  days. Contour interval is 10 m.

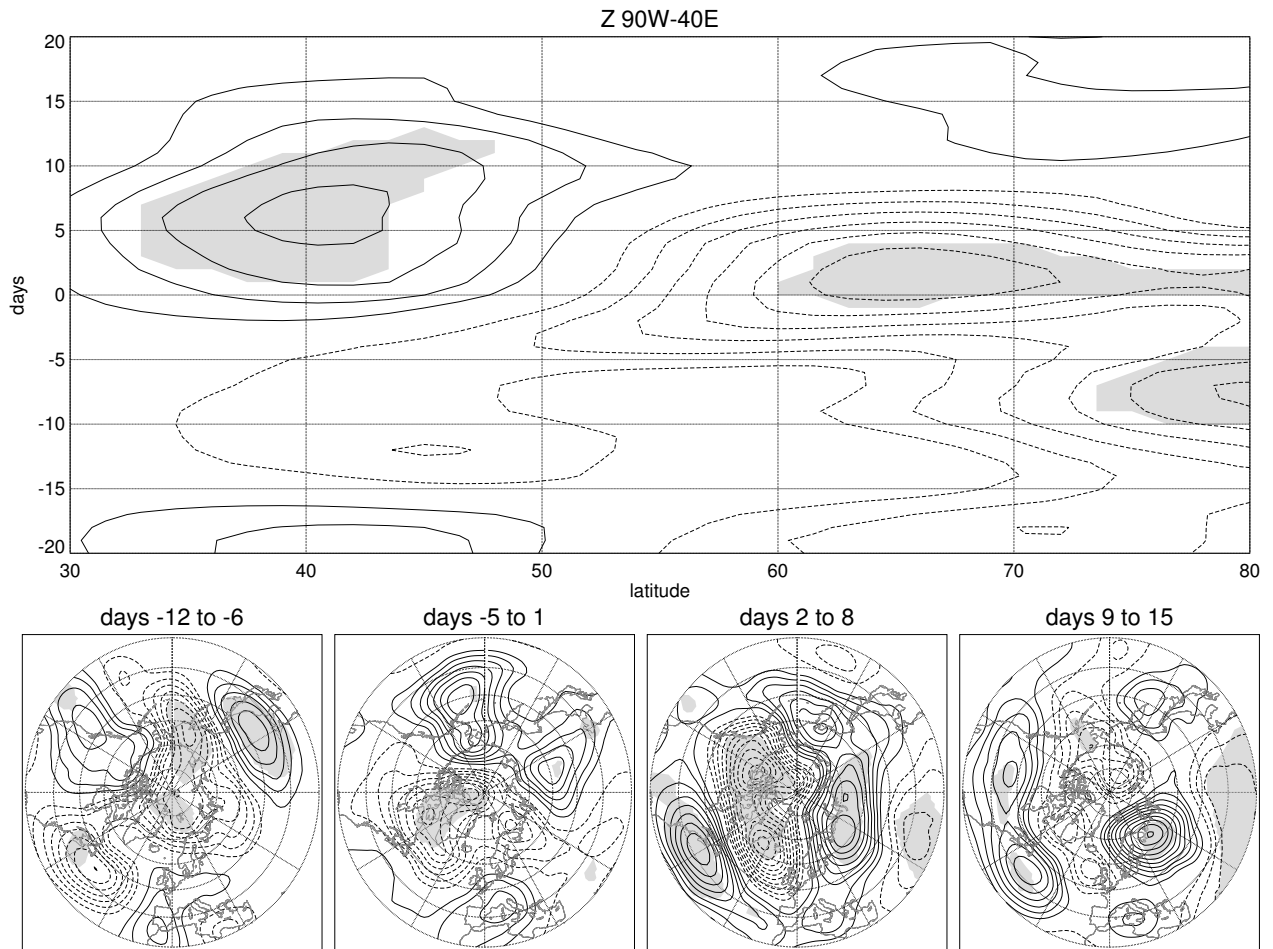


FIG. 6. Top: The evolution of the 500 hPa geopotential height anomaly averaged from  $90^{\circ}\text{W}$  to  $40^{\circ}\text{E}$  for the composite downward wave coupling event as a function of time from  $-20$  to  $20$  days and latitude. Bottom: The 500 hPa geopotential height anomaly averaged from  $-12$  to  $-6$ ,  $-5$  to  $1$ ,  $2$  to  $8$  and  $9$  to  $15$  days. Contour interval is  $10$  m. Shading indicates statistical significance at the  $95\%$  level based on a t-test.

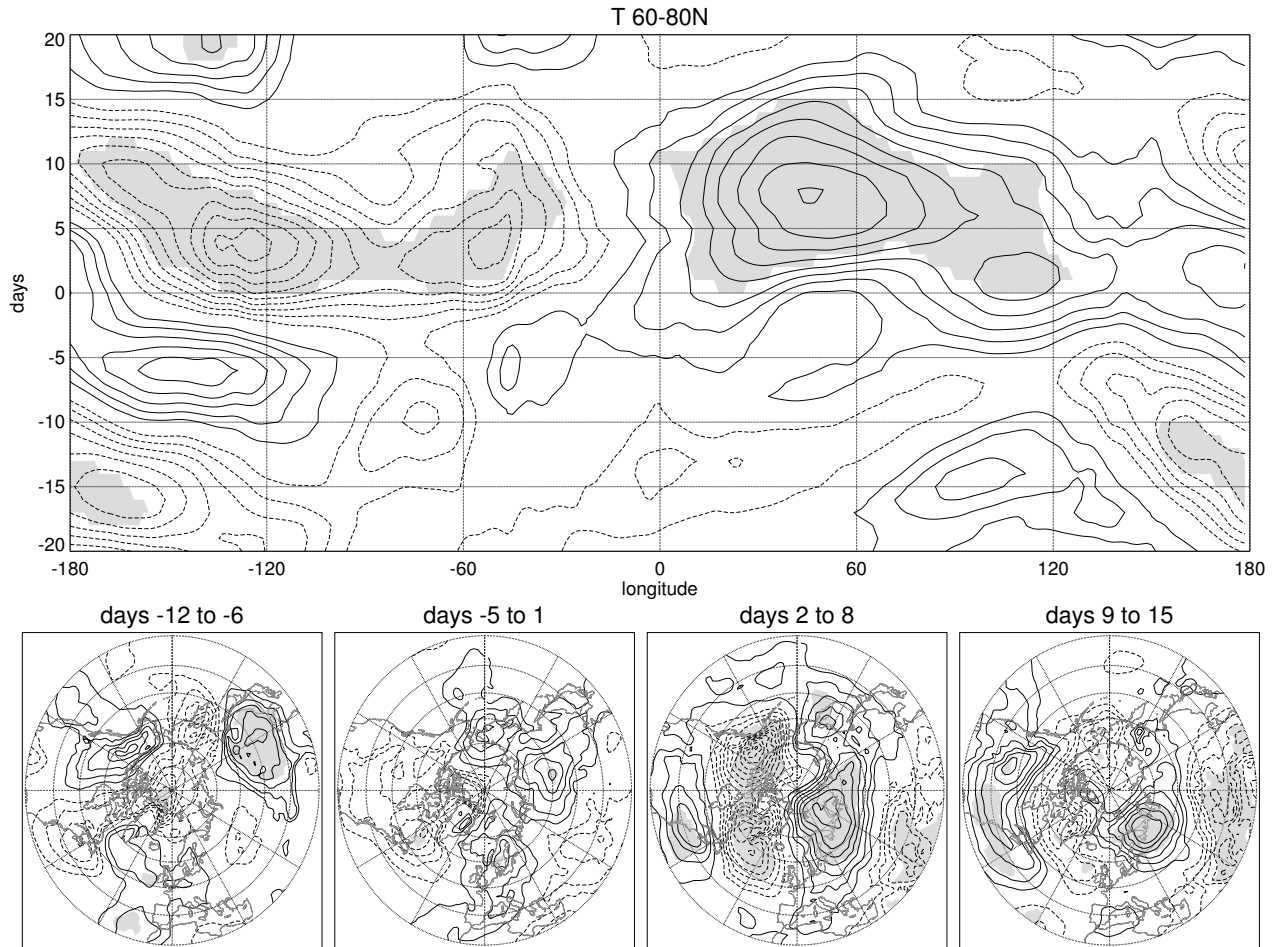


FIG. 7. Top: The evolution of the 850 hPa temperature anomaly averaged from 60 to 80°N for the composite downward wave coupling event as a function of time from  $-20$  to  $20$  days and longitude. Bottom: The anomalous 850 hPa temperature averaged from  $-12$  to  $-6$ ,  $-5$  to  $1$ ,  $2$  to  $8$  and  $9$  to  $15$  days. Contour interval is  $0.5$  K. Shading indicates statistical significance at the 95% level based on a t-test.

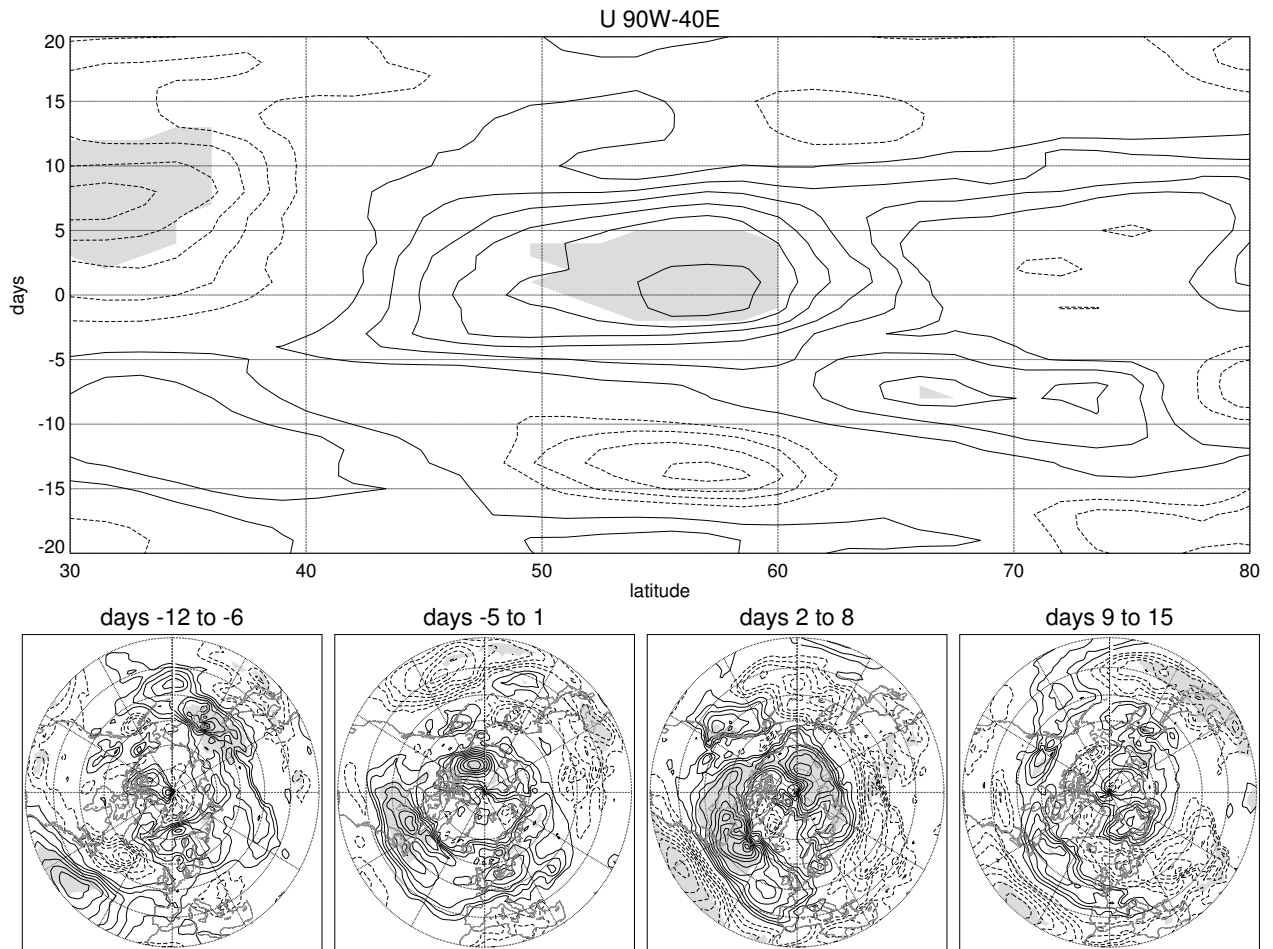


FIG. 8. Top: The evolution of the 850 hPa zonal wind anomaly averaged from  $90^{\circ}\text{W}$  to  $40^{\circ}\text{E}$  for the composite downward wave coupling event as a function of time from  $-20$  to  $20$  days and latitude. Bottom: The anomalous 850 hPa zonal wind averaged from  $-12$  to  $-6$ ,  $-5$  to  $1$ ,  $2$  to  $8$  and  $9$  to  $15$  days. Contour interval is  $0.5 \text{ ms}^{-1}$ . Shading indicates statistical significance at the 95% level based on a t-test.

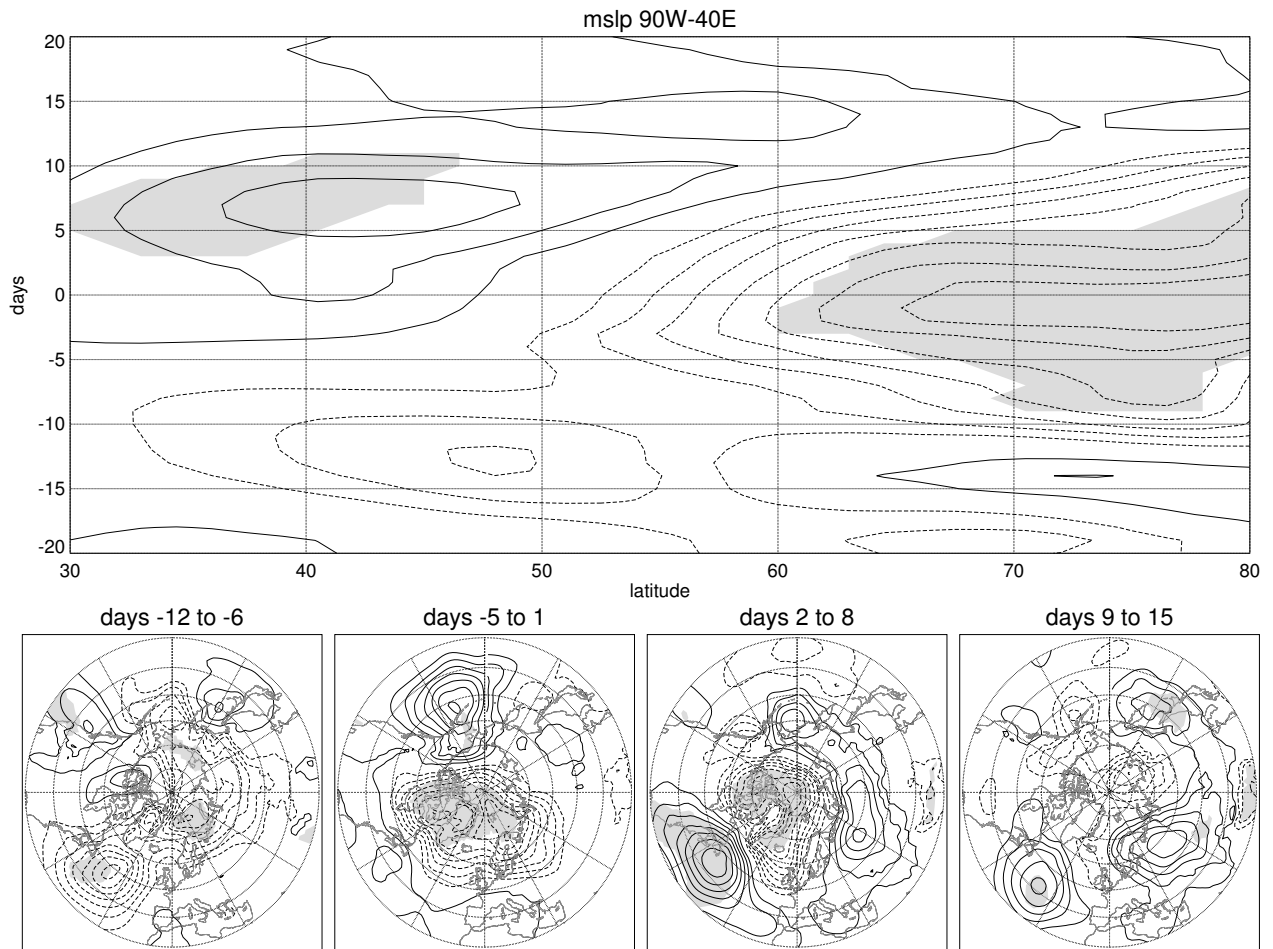


FIG. 9. Top: The evolution of the mean sea level pressure anomaly averaged from  $90^{\circ}\text{W}$  to  $40^{\circ}\text{E}$  for the composite downward wave coupling event as a function of time from  $-20$  to  $20$  days and latitude. Bottom: The anomalous mean sea level pressure averaged from  $-12$  to  $-6$ ,  $-5$  to  $1$ ,  $2$  to  $8$  and  $9$  to  $15$  days. Contour interval is  $1$  hPa. Shading indicates statistical significance at the  $95\%$  level based on a t-test.

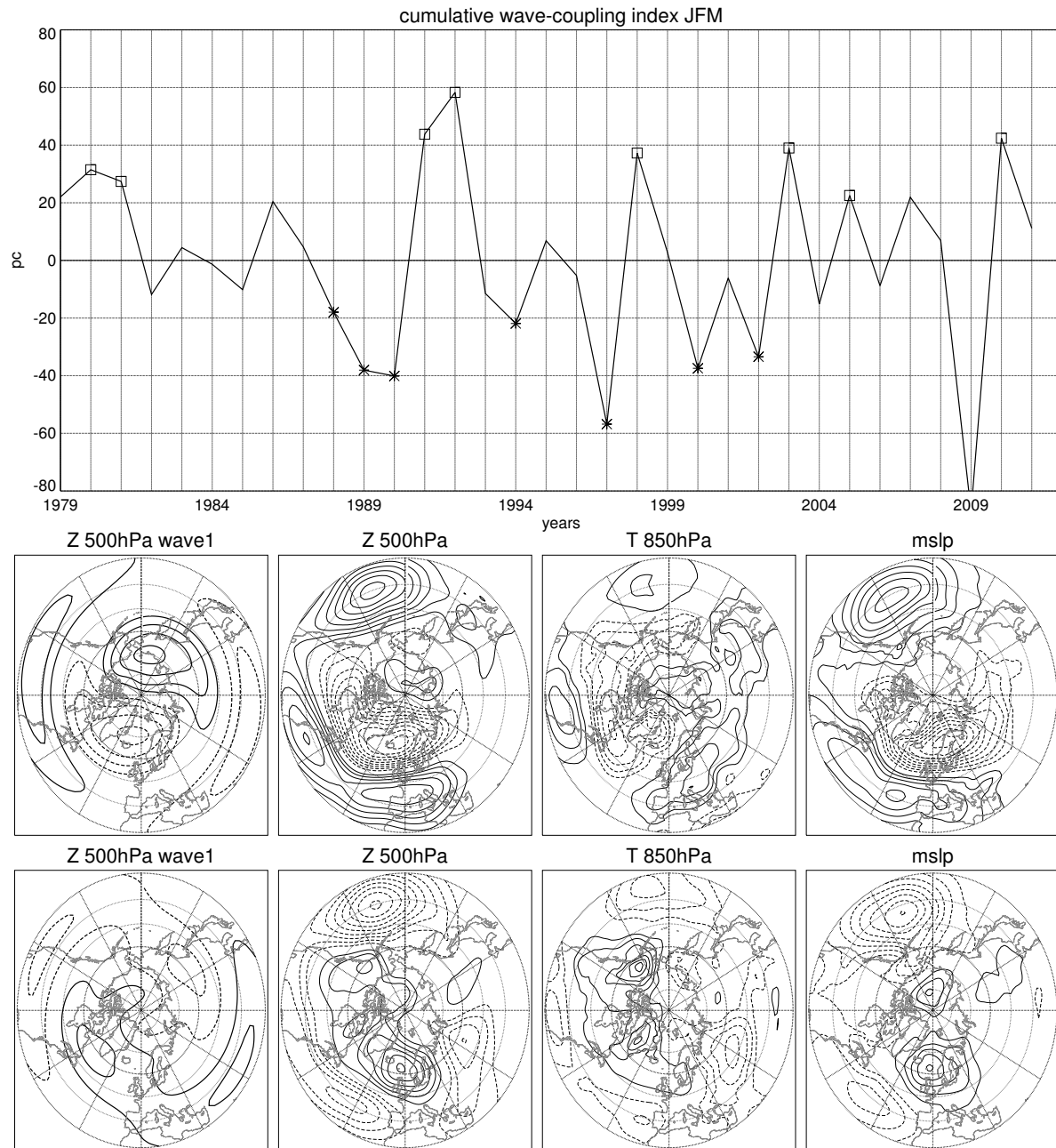


FIG. 10. Top: Sum of the JFM wave-coupling index (leading pc of the wave-1 flux at 30 hPa) as a function of year. Middle: The 500 hPa wave-1, the 500 hPa geopotential height, the 850 hPa temperature and the mean sea level pressure anomalies during years with a star. Bottom: Same as middle but for years with a square. Contour interval is 5 m for 500 hPa wave-1 and 500 hPa geopotential height anomalies, 0.25 K for 850 hPa temperature anomaly and 0.5 hPa for mean sea level pressure anomaly.

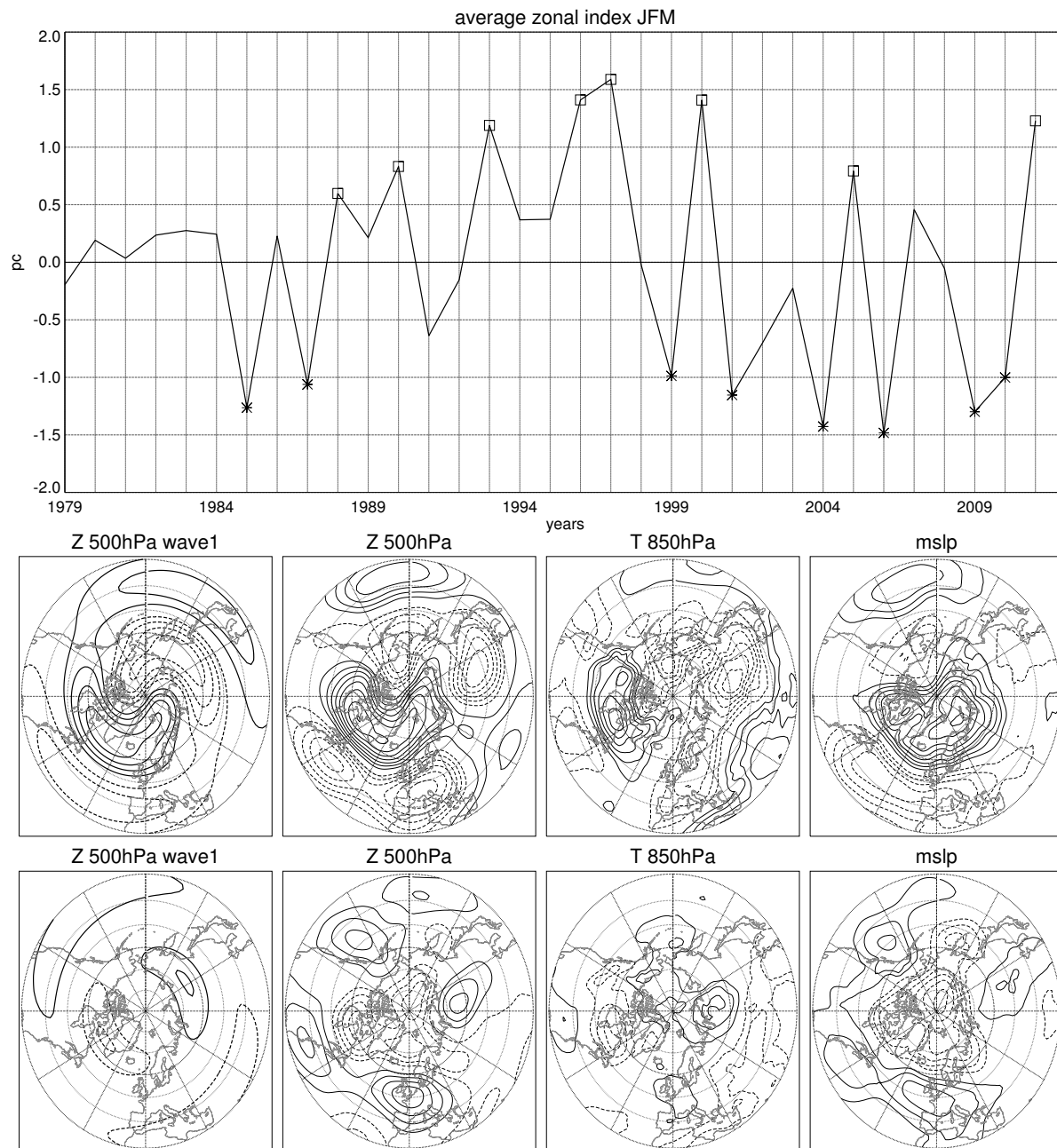


FIG. 11. Top: The JFM average zonal-index (leading pc of the zonal-mean geopotential at 30 hPa) as a function of year. Middle: The 500 hPa wave-1, the 500 hPa geopotential height, the 850 hPa temperature and the mean sea level pressure anomalies during years with a star. Bottom: Same as middle but for years with a square. Contouring as in Fig. 10.